Journal of Electronics, Electromedical Engineering, and Medical Informatics
Homepage: jeeemi.org; Vol. 8, No. 4, October 2026, pp: 1331-1353 e-ISSN: 2656-8632

RESEARCH ARTICLE OPEN ACCESS

Electrooculography-Based Voluntary Eye-Blink Detection for Arabic Assistive Communication

Afrah Thamer, and Musaab Alaziz

Department of Computer Engineering, College of Engineering, University of Basrah, Basrah, Iraq

Corresponding author: Afrah Thamer (e-mail: afrah.dhamid@uobasrah.edu.iq), **Author(s) Email**: Musaab Alaziz (e-mail: mosab.adil@uobasrah.edu.iq)

Abstract **People with profound neuromotor disabilities commonly experience significant speech disability and lack of voluntary control over their limbs, retaining, however, the ability to perform deliberate eyelid blinks. Such retained capability presents an opportunity to be used as assistive communication. Nevertheless, reliable detection of voluntary blinks and decoding of communication patterns based on them is challenged by variation in the waveforms, amplitudes, durations, and inter-blink intervals of the voluntary eye blinks. In this work, a cost-efficient vertical electrooculography (EOG) approach for detecting voluntary eye blinks and decoding predefined assistive messages in Arabic was presented and assessed. The pipeline consists of signal conditioning, root-mean-square envelope calculation, adaptive hysteresis-based thresholding, temporal segmentation, and rule-based interpretation of single- and double-blink patterns. Quiet-background threshold updating and locking it during the communication window period were used to increase the robustness of the pattern detection process, while autocorrelation analysis and temporal constraints were utilized to interpret patterns. A single blink is associated with binary 0, and a double blink with binary 1; four consecutive pattern positions form a 4-bit frame that represents one of sixteen predefined Arabic messages. Unclear patterns are excluded from processing and not mapped into any valid message. The proposed approach was evaluated offline on 4,000 word-level recordings from 25 healthy participants, with verification using videos. The F1-score of 95.69%, macro-F1-score of 98.30%, and message-decoding accuracy of 92.98% were obtained. These findings demonstrate the possibility of implementing an interpretable and cost-efficient vertical-EOG approach for message-level Arabic assistive communication without morse-code-type encoding and letter-by-letter spelling. Direct mapping of patterns into messages can help reduce communication effort and time. Nevertheless, since the present evaluation was conducted offline and included only healthy subjects, further validation with target users and real-time implementation should be conducted before deployment.**

Keywords **Electrooculography (EOG); Biomedical Signal Processing; Adaptive Thresholding; Single/Double Blink; Binary Encoding; Arabic Assistive Vocabulary**

I. Introduction

This work considers the interface needs of persons with severe neuromuscular disorders who have lost speech and voluntary limb functions, yet retain certain ocular abilities, e.g., partial eye movements and voluntary blinks. In this situation, AAC systems become an important means of communicating basic needs and interacting with caregivers [1], [2], [3], [4]. Blink-based communication is a very promising solution for its simplicity, independence from limb movement, and voluntary production capabilities in cases of severe motor disorders [5], [6]. At the same time, reliable blink-based interaction requires precise detection and temporal segmentation, since imprecision in blink onset, offset, duration, and location can carry over to the interpretation stage and lead to incorrect message interpretation.

Assistive eye-focused interaction can be done via camera-based eye tracking, BCIs, EEG, and EOG. Camera- and gaze-based solutions provide useful interaction channels, yet they are sensitive to illumination conditions, eyelid visibility, head pose, calibration procedures, and computation requirements [7], [8]. Moreover, EEG- and BCI-based interaction tools can facilitate communication, especially when neural activity or evoked responses serve as input. As for voluntary blink input, blink activity is usually estimated from frontal EEG channels, such as FP1, where ocular artifacts appear as high-amplitude events in the brain signal recordings [9], [10]. On the other hand, vertical EOG provides direct recording of corneo-retinal potential changes during eye movements and blinking, therefore, represents a cheap and physiologically relevant tool for blink-based assistive

Manuscript received 13 May 2026; Revised 20 July 2026; Accepted 30 July 2026; Available online 10 August 2026
Digital Object Identifier (**DOI**): https://doi.org/10.35882/jeeemi.v8i4.1848

interaction [11], [12], [13], [14], [15], [16], [17], [18], [19], [20], [21], [22], [23], [24], [25], [26], [27].

Previous studies of blink-based communication show that voluntary blinks can be associated with letters, words, commands, or speech. For Morse code and letter-level encoding schemes, characters can be encoded as blinks and pauses; however, these approaches may require several blinks and pause periods to transmit a single character or an entire message [9], [28], [29], [30]. Other works use machine learning and similarity-based methods to discriminate among single, double, and triple blinks, or to map binary blink patterns to specific expressions [31], [32]. However, these studies highlight not only the potential for low-cost blink-based communication but also challenges with blink burden, temporal segmentation, signal modality, and message-level reliability.

Despite advances in the field, detection-centered Arabic blink communication using a dedicated vertical EOG channel remains scarce. In particular, the closest blink-to-speech systems usually infer blink activity from frontal EEG/FP1 recordings or use Morse-like and letter-level spelling schemes, which can increase blink burden and communication time. Although predefined-message coding can help reduce burden, no work combines direct vertical-EOG signal acquisition, stable voluntary-blink segmentation, interpretable single- or double-blink pattern interpretation, and Arabic message decoding within a single evaluated pipeline. Thus, there is a need for a low-cost, interpretable vertical-EOG solution to assist Arabic communication at the level of predefined messages rather than single letters.

To address this problem, this paper proposed and evaluated a vertical-EOG detection pipeline for voluntary eye-blink analysis in Arabic assistive communication. The pipeline comprises signal conditioning, RMS envelope estimation, adaptive blink detection, quiet-background threshold updating, threshold locking within the message window, rule-based interpretation of single- and double-blink patterns, and four-bit Arabic message decoding. The work focuses on the detection and temporal interpretation stages, where precise blink segmentation is essential for reliable message decoding. The pipeline was tested offline on 4,000 word-level recordings from 25 healthy subjects, and performance was assessed at the blink-detection, blink-pattern interpretation, and message-decoding levels.

The main contributions of the work can be formulated as follows:

1. Detection-centered vertical-EOG framework for voluntary eye-blink analysis in Arabic assistive communication, providing a direct ocular-signal alternative to blink extraction from frontal EEG channels.
2. Stable blink-segmentation scheme developed using RMS-envelope analysis, quiet-background threshold updating, hysteresis thresholding, and threshold locking during the communication window.
3. Interpretable single- or double-blink-pattern interpretation stage designed based on temporal constraints and supported by autocorrelation and peak validation rules.
4. Four-bit Arabic message-decoding layer that maps validated blink-pattern sequences to sixteen predefined assistive messages, thereby avoiding Morse code and letter-by-letter spelling.
5. Multi-level offline evaluation was conducted at the blink detection, blink pattern interpretation, and message decoding levels, using 4,000 word-level recordings from 25 healthy subjects.

The rest of the paper was organized as follows. Section II presents the EOG signal acquisition system, data acquisition methodology, preprocessing, adaptive blink detection, blink pattern analysis, and Arabic message decoding. Section III discusses the results and conclusions, including a multi-level performance analysis, a comparison with related literature, limitations, and suggestions for further work. The final section concludes the paper.

II. Method

A. Overview and EOG Signal Acquisition Setup

The proposed architecture was designed to measure voluntary eye-blink activity via the vertical EOG channel and to use this signal as the physiological input for decoding assistive Arabic messages. As depicted in Fig. 1, the measurement acquisition path starts in the periocular area, where a voluntary blink generates a temporary change in the corneo-retinal potential. Since the cornea is positively charged relative to the retina, eyelid closure and eye movement produce a small electrical difference that can be measured on the skin around the eye [9], [15], [16]. For this reason, two surface Ag/AgCl electrodes were placed vertically on the top and bottom of one eye to measure the blink activity-related differential EOG signal, with an additional reference electrode positioned behind the ear. To improve skin-electrode contact and reduce contact impedance, Ten20 conductive gel was used. The aforementioned vertical arrangement of the electrodes was adopted because blink activity primarily reflects the vertical component of the EOG, and it aligns with human-computer interaction EOG-based architectures and assistive recordings [9], [15], [16], [25], [31].

The generated periocular biopotential is weak and prone to baseline drift, electrode contact variability, and ambient noise. Hence, the differential EOG signal was fed into the BioAmp EXG Pill, which served as the analog front-end for biopotential amplification and initial

Manuscript received 13 May 2026; Revised 20 July 2026; Accepted 30 July 2026; Available online 10 August 2026
Digital Object Identifier (**DOI**): https://doi.org/10.35882/jeeemi.v8i4.1848

signal conditioning. The analog-conditioned EOG signal was then input into the analog input of the Arduino UNO R4 and sampled at 60 Hz. The obtained digital signal samples were sent to MATLAB through the USB serial port for storing and further offline processing. In MATLAB, the recorded signal was preprocessed, its RMS envelope was created, adaptive blink detection was performed, the signal was temporally segmented, blink patterns were interpreted according to rules, and the four-bit Arabic message was decoded. Therefore, Fig. 1 shows the vertically integrated signal-flow architecture of the proposed assistive communication system based on EOG signal processing. The EOG signal from the periocular area is obtained using the electrodes and BioAmp EXG Pill, which then converts the signal into digital form using the Arduino UNO R4 and sends the data to MATLAB for offline analysis. Preprocessing, blink detection, double-blink detection, and message decoding operations were all carried out within the MATLAB environment, and hence, the blinks can be mapped into an Arabic message.

level evaluation dataset utilized to measure fixed system performance.

In this case, the division into calibration and evaluation data was motivated by the natural variations of voluntary blinks. Although the same participant was performing the same blink task, the amplitude, duration, sharpness, completeness, and inter-blink timing of the resulting EOG waveform might vary because of individual physiological characteristics, blink effort, attention, fatigue, and unstable electrode-skin contact. As such, calibration recordings were applied to determine the stable preprocessing, detection, segmentation, and interpretation parameters before the evaluation test, while the final evaluation dataset was analyzed without any further modification of these parameters.

The calibration recordings were recorded from 25 subjects who were not included in the final evaluation group. For each calibration subject, a two-minute recording of voluntary single- and double-blink responses was recorded. These recordings were not arranged as Arabic message trials and contained no

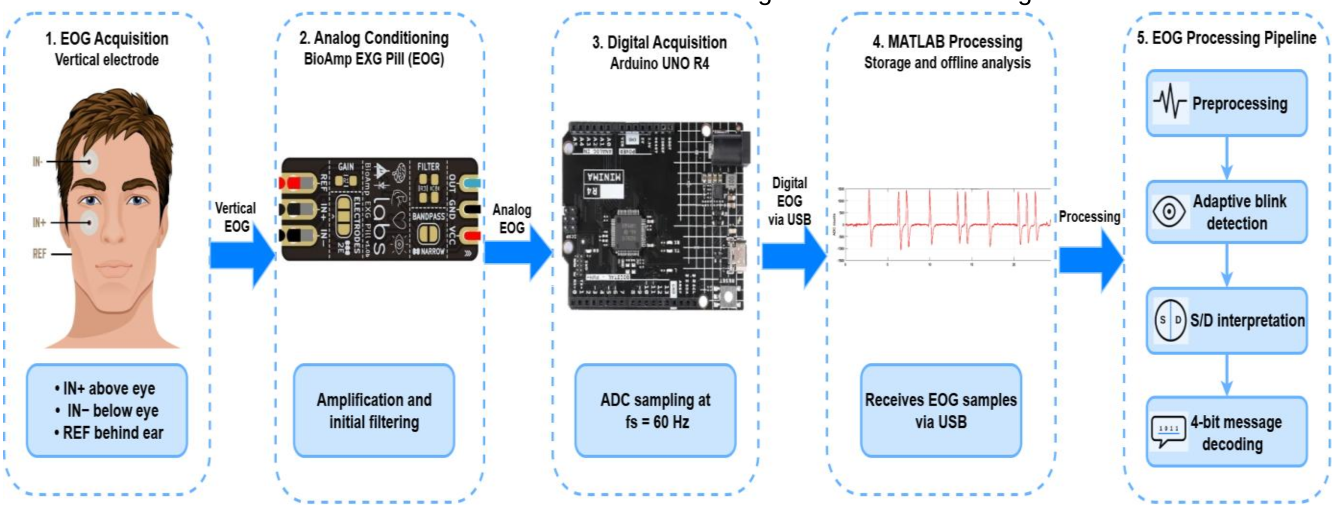

Fig. 1. Proposed Vertically Integrated EOG-Based Assistive Communication System Architecture: The above diagram shows the full signal flow from the beginning to the end, starting with the acquisition of periocular electrodes and extending through 4-bit message decoding.

B. Dataset and Data Acquisition Protocol

The experimental data were recorded according to the standard electro-oculography (EOG) protocol that was designed for the development and evaluation of a voluntary blink-based Arabic assistive communication pipeline. The acquisition setup described in Fig. 1 remained unchanged throughout all recordings to ensure electrode configuration, signal acquisition, and data transfer consistency. Recorded data were further divided into two independent parts: calibration recordings necessary for determining the numerical parameters of the processing pipeline and the word-four-bit word frames; instead, they were used to describe the simple voluntary blinks that serve as a basis for communication protocol design. After being verified through manual inspection, the calibration recordings were used to define the fixed parameters of the proposed pipeline, including preprocessing, RMS-envelope construction, adaptive threshold control, event segmentation, single/double blink interpretation, and rejection rules, as summarized in Table 1. Once defined, these parameters were kept unchanged and used without any modifications in the evaluation dataset.

The independent evaluation dataset was recorded from 25 healthy adult volunteers, including 10 men and

Manuscript received 13 May 2026; Revised 20 July 2026; Accepted 30 July 2026; Available online 10 August 2026
Digital Object Identifier (**DOI**): https://doi.org/10.35882/jeeemi.v8i4.1848

15 women, aged 20–64 years. The inclusion criteria were understanding the experimental instructions, maintaining a comfortable seated position during acquisition, and intentionally performing the specified single- and double-blink sequences. The exclusion criteria were uncontrollable eyelid tremor, involuntary blink sequences that interfered with the target pattern, inability to vary voluntary blink responses, and any other condition that made the task difficult to perform. No clinical users were involved in this phase. Participants had normal or corrected-to-normal vision, and some of them wore glasses due to myopia.

Before each recording session, the electrode placement sites were cleaned to increase the stability of electrode-skin contact. The participants were asked to refrain from head and facial movements during acquisition, taking breaks when necessary to reduce fatigue. Each participant performed 16 predefined Arabic assistive messages, and each message was repeated 10 times, providing an evaluation dataset consisting of 160 word-level recordings per participant and 4,000 word-level recordings in total. Each recording corresponds to an attempt to convey the target message using the four-bit blink sequence, with each bit corresponding to a specific temporal pattern slot. A voluntary single blink corresponds to binary "0," while a voluntary double blink corresponds to binary "1." The correspondence between the four-bit frames and the respective Arabic assistive messages is summarized in Table 2.

The EOG signals were sampled at a frequency of 60 Hz, providing a temporal resolution of 16.7 milliseconds between consecutive samples. This sampling frequency is a good compromise between temporal resolution, signal stability, and low-cost acquisition. Given that voluntary blinks last for hundreds of milliseconds, a single-blink event can be represented by multiple samples, while a double-blink response takes longer. The bandwidth of the preprocessing filter is limited to frequencies lower than the Nyquist frequency (30 Hz), with the upper frequency limit of 15 Hz. Thus, the sampling rate provides sufficient temporal resolution to estimate the onset, offset, duration, and inter-blink timing of blink responses within the proposed rule-based pipeline. In addition, blink segmentation does not rely on the isolated threshold crossing of a single sample; it uses RMS-envelope smoothing, hysteresis thresholding, onset-validation timing, refractory control, and calibration-based temporal decision rules.

The ground-truth labeling was performed using the protocol-defined and video-verified procedure. During evaluation recordings, a fixed camera verifies the participant's performance of the required blink pattern. For each trial, the target Arabic message and its corresponding four-bit blink sequence are predefined by the acquisition protocol. Arduino-generated markers indicate the word window and four pattern windows, providing the possibility to align and construct the ground-truth tables. These markers were used exclusively for synchronization and evaluation table construction purposes and were not used as features by the proposed EOG detection algorithm. The camera recordings were inspected manually after acquisition to make sure that the executed blink sequence matches the target blink pattern. Trials containing technical errors, problems with markers, incorrect acquisition conditions, or ambiguous blink execution were repeated before being included in the analysis. As such, the final evaluation dataset contains 4, 000 video-verified word-level recordings. The inter-rater reliability was not estimated, as the manual verification was performed by a single reviewer.

C. Pipeline Standardization and Parameter Calibration

The approach applied is based on a standard end-to-end EOG processing pipeline, which was calibrated in order to convert the measured vertical EOG signal into an assistive decoded Arabic message. At each run, there was always a constant sequence of steps, such as signal capture, preprocessing, RMS envelope estimation, adaptive blink detection and segmentation, interpretation of single and double blinks using rules, and decoding of four-bit messages. Calibration runs were performed to characterize the blink units, which were used as building blocks for the communication protocol—namely, single isolated blinks and double blinks. It is important to mention that we do not consider the word-level frames in the Arabic language in our calibration set. Using these data, the thresholds and other parameters were derived for signal conditioning, envelope extraction, thresholding, validation, grouping, waveform comparison, and invalid response rejection. The fixed acquisition setup and message coding approach remained constant during the whole experiment. The values of the calibration-derived parameters were fixed before the processing of the independent word-level test set. Table 1 summarizes the stage-wise organization of the proposed pipeline, including the corresponding setting or parameter, its fixed value, and its functional role.

D. Signal Preprocessing

Electrooculogram (EOG) signals have often been affected by baseline drifts, electrode-skin interface drifts, impulses, and high-frequency noises. For this reason, the preprocessing procedure has been developed to condition the signal while maintaining the temporal morphology of the blink response [18]. First, the mean value of the signal has been subtracted in order to compensate for the DC bias created in the

Manuscript received 13 May 2026; Revised 20 July 2026; Accepted 30 July 2026; Available online 10 August 2026
Digital Object Identifier (**DOI**): https://doi.org/10.35882/jeeemi.v8i4.1848

Journal of Electronics, Electromedical Engineering, and Medical Informatics
Homepage: jeeemi.org; Vol. 8, No. 4, October 2026, pp: 1331-1353 **e-ISSN: 2656-8632**

Table 1 Key standardized settings and calibration-derived parameters of the proposed EOG blink-based communication pipeline

Stage	Parameter\Symbol	Value	Functional role
Acquisition	Electrode placement	Above and below one eye	Vertical EOG recording
	Reference electrode	Behind the ear	Stable EOG reference
	Sampling rate f_s	60 Hz	16.7 ms blink-timing resolution
Preprocessing	Band-pass filter	0.2–15 Hz	Retains blink-related EOG activity
	Filter type/order	2nd-order Butterworth	Fixed signal conditioning
	RMS window	0.20 s	Smooths blink-energy envelop
Adaptive Blink Detection and Temporal Segmentation	Baseline interval	5.0 s	Estimates the initial quiet-envelope level
	Background buffer	6.0 s	Stores recent quiet samples
	Threshold update interval	0.25 s	Updates threshold during quiet periods
	Threshold-locking window	20.0 s	Prevents threshold drift during message window
	K_{on}	11	Onset hysteresis multiplier
	K_{off}	5	Offset hysteresis multiplier
	t_{val}	0.12 s	Rejects short activations
	t_{ref}	0.10 s	Prevents duplicate detections
	α	0.30	Controls adaptive event termination
Blink-pattern Interpretation	d_i	0.3404 – 0.8531 s	Accepted single-blink duration
	g_i	0.2400 – 0.7667 s	Accepted inter-blink gap
	Δ_i^D	0.9208 – 2.4729 s	Accepted double-blink span
	A_S	0.471 – 0.864	Single-blink waveform consistency
	A_D	0.148 – 0.431	Double-blink waveform consistency
	r_H	0.25 (25%)	Peak-height validation ratio
Message decoding	Bit assignment	S = 0, D = 1	Converts pattern to bit
	Message frame	4 bits Encodes	16 Arabic messages

analog front-end and electrode-skin interface. Robust local median correction has been employed in order to compensate for the impulses. In this step, all signal samples showing a significant deviation from the trend of the local signal have been replaced with the respective median value, which allows minimizing the effect of electrode movement or cable instability on the blink signal without considerable distortion of the signal.

After noise reduction was completed, a second-order Butterworth band-pass filter was used with passband frequencies ranging between 0.2 and 15 Hz. This filtering layer was used to minimize very low frequency baseline drift and high frequency noise while preserving the low frequency temporal morphology of the voluntary EOG blink responses [11], [12], [13], [25], [33]. To verify the appropriateness of the bandpass range chosen, spectral power analysis was performed on the independent calibration recordings from 25 subjects who voluntarily blinked, applying the Welch method of estimation. The mean value of the ratio of the band energy to the total energy in the selected 0.2–15 Hz frequency range was 97.3% with a standard deviation of 1.5%, a median of 97.9%, and an interquartile range of [96.3%, 98.3%], which shows that most of the spectral energy due to blinks is preserved in the selected band. Finally, the band-pass filtered blink signal was converted to a positive representation by instantaneous power estimation, smoothed with moving averages, and then enveloped in RMS, which was used in the subsequent adaptive detection stage.

E. Adaptive Blink Detection and Temporal Segmentation

The RMS envelope served as the detection signal, transforming blink-related EOG activity into a continuous positive-energy representation that minimized polarity-dependent waveform fluctuations. The detection stage was developed to extract temporally consistent blink segments, as reliable voluntary blink interpretation relies on stable start, offset, and duration prediction, rather than simply identifying local amplitude peaks [18]. This is especially significant in voluntary blink-based engagement, where blinks are deliberately employed as control events. The static global threshold was overcome due to the presence of variations in EOG signal amplitude and background noise for each subject and measurement session [34], [35]. The thresholding system calculated

Manuscript received 13 May 2026; Revised 20 July 2026; Accepted 30 July 2026; Available online 10 August 2026
Digital Object Identifier (**DOI**): https://doi.org/10.35882/jeeemi.v8i4.1848

Journal of Electronics, Electromedical Engineering, and Medical Informatics
Homepage: jeeemi.org; Vol. 8, No. 4, October 2026, pp: 1331-1353 e-ISSN: 2656-8632

the baseline locally using the quiet-background samples. These samples were used to estimate the local baseline envelope $\widetilde{e_q}(n)$,and the local variability $\sigma_q(n)$ terms were determined using three timing parameters derived from the calibration procedure and given in Table 1. At the beginning of each recording, the 5.0-second-long quiet baseline interval was recorded before the first deliberate blink event. During this interval, the subject was asked to relax and not to blink involuntarily so that the RMS envelope measured would represent only the resting background EOG activity. The initial interval was used to initialize the quiet-background median $\widetilde{e_q}(n)$ and variability $\sigma_q(n)$. In further processing, the 6.0-second-long quiet-background buffer consisted of recently acquired envelope samples that were not assigned to active blink periods, and the baseline statistics were estimated every 0.25 seconds when the system was in the quiet state. This method is based on the vulnerability of EOG records to slow baseline drift, variations in the contact of electrodes with the skin, and other sources of noise that are not related to blink events. Estimating the background only during quiet periods allowed the adaptive thresholds to follow slow background variations while preventing blink-related energy from contaminating the background estimate [13], [36]. The resulting background estimates were then used to set hysteresis-based thresholds for blink onset and offset detection. Eq. (1) and Eq. (2) were defined in this study as a calibration-derived adaptive thresholding rule, while the general use of adaptive threshold estimation is consistent with previous eye-event detection methods. These thresholds were calculated based on Eq.(1), Eq.(2) [37]:

$$T_{on}(n) = \widetilde{e_q}(n) + K_{on}\sigma_q(n) \tag{1}$$

$$T_{off}(n) = \widetilde{e_q}(n) + K_{off}\sigma_q(n)\ , K_{on} > K_{off} \tag{2}$$

In discrete time, n denotes the sample index. The thresholds $T_{on}(n)$ and $T_{off}(n)$ are applied to the RMS envelope to compute the activation and release conditions for a proposed blink event. The $\widetilde{e_q}(n)$ denotes the local median of the quiet-background RMS envelope, whereas $\sigma_q(n)$ represents the corresponding local variability estimate, and the subscript q was used here to denote time epochs without detected blink events. This approach allows tracking the threshold with slow changes in the baseline while maintaining the dynamic behavior of the envelope caused by voluntary blinks. Since the EOG was first transformed into units of millivolts, the values of $T_{on}(n)$, $T_{off}(n)$, $\widetilde{e_q}(n)$ and are $\sigma_q(n)$ are expressed in millivolts (mV), while K_{on} and K_{off} are dimensionless hysteresis multipliers. The inequality $K_{on} > K_{off}$ leads to the hysteresis of the activation and release of an event. The hysteretic multipliers were experimentally estimated from the independent calibration dataset and remained constant before applying the proposed pipeline to the final evaluation dataset at the word level. The selected values for K_{off} and K_{on} are listed in Table 1. These multipliers have been selected to maintain a distinct hysteresis gap between the offset and onset thresholds, minimizing false detections from baseline noise fluctuations while retaining genuine voluntary blink events. Calibration of these multipliers is essential because EOG signals are susceptible to amplitude variations due to inter-subject variability, baseline shifts, electrode contact, and noise. Upon the detection of the initial sustained valid activity, the existing threshold values were secured for a 20-second communication interval. The threshold-locking strategy expressed in Eq. (3) was proposed in this study to prevent repeated voluntary blinks from contaminating the quiet-background estimate during the active communication window.

$$T_j(n) = T_j(n_0), \in j\{on, off\}, \quad t_{n_0} \le t_0 \le t_{n_0} + 20s \tag{3}$$

where n_0 represents the first sample corresponding to the first sustained blink activity, and $j \in \{on\ , off\}$ was used to show that both onsets and offset thresholds were locked. The idea behind locking is that repeated voluntary blinking might increase the background-level estimate and reduce the ability to detect blinks. The 20s lock-in threshold window was selected according to the four-position message protocol and confirmed using the calibration recordings from 25 subjects, such that it included the longest possible communication frame consisting of four double-blinks and the delay intervals between them [13]. The candidate blink events were detected using the state detector rather than simple threshold crossings. A valid onset was defined when the RMS envelope was still above $T_{on}(n)$ for a certain validation time period, thus eliminating any short-term deviations from the envelope that could be classified as blink events. After a successful event, the detector would enter a short refractory period before detecting a new candidate. The refractory period ensures that the leftover tail, or residual, of the previous blink event is not re-detected as another blink event. The parameters used here for the onset-validation period and the refractory period were calibrated and set before analysis and are provided in Table 1. After satisfaction of the onset-validation condition, the candidate was considered an instance of an active blink event. For the determination of its endpoint, an adaptive end-level, $E_{end}(n)$, was defined in this study as a peak-dependent event-termination rule, as given in Eq.(4):

$$E_{end}(n) = \max(T_{off}(n), \widetilde{e_q}(n) + \alpha \max(e_{peak} - \widetilde{e_q}(n), 0)) \tag{4}$$

The blink event would end once the RMS envelope, e(n), fell below the level $E_{end}(n)$. This adaptive end level is a combination of two criteria – the adaptive offset threshold, $T_{off}(n)$, and peak-dependent decay level based on the current amplitude of the blink. In

Manuscript received 13 May 2026; Revised 20 July 2026; Accepted 30 July 2026; Available online 10 August 2026
Digital Object Identifier (**DOI**): https://doi.org/10.35882/jeeemi.v8i4.1848

Journal of Electronics, Electromedical Engineering, and Medical Informatics
Homepage: jeeemi.org; Vol. 8, No. 4, October 2026, pp: 1331-1353 e-ISSN: 2656-8632

Eq.(4), $\widetilde{e_q}(n)$ represents the median value of the envelope during the quiet background period, whereas e_{peak} refers to the maximal value of the RMS envelope during the current event. The parameter α determines the influence of the current amplitude of the blink on the ending level. In this study, the value of α was set experimentally for the calibration dataset and kept constant during the testing process, as described in Table 1. The duration of the blink event number i was computed from its detected onset and offset times, since blink duration and event boundaries are essential for blink characterization, as shown in Eq.(5) [18]:

$$d_i = t_{off}^{(i)} - t_{on}^{(i)} \quad (5)$$

where $t_{on}^{(i)}$ and $t_{off}^{(i)}$ represent the time of occurrence and end time of the i-th detected blink event, respectively, while d_i represents the blink duration of the i-th blink event in seconds. The segmented blink events were then sent to the next rule-based interpretation stage as the unit candidates. Fig. 2 shows the entire blink extraction process for the suggested adaptive detection process. First, the band-pass EOG signal is converted to an RMS envelope to obtain a stable positive form of the blink events. Onset and offset thresholding is then performed on the envelope using the threshold lock window to avoid drift of the threshold value within the period of active communication. As such, the output of the detector will be the state-based binary mask where the onset and offset of each blink event are determined precisely. The onset and offset values determine the temporal span of each blink and provide the segments that will be classified in the rule-based phase.

F. Rule-Based Interpretation of Single and Double Blink Sequences

After the identification and temporal segmentation of the adaptive blink, the verified blink segments then passed through a rule-based interpretation process to interpret blink sequences into classes rather than directly transforming them into communication commands. At this stage, the blink segments were transformed into binary digits, which served as input for the four-bit message Arabic decoder. A single blink is considered digit 0, while a double blink represents digit 1, with questionable candidates being labeled as unknown (U). This is an important step, as communication using blinks involves detecting as well as differentiating individual voluntary blinks. Due to the effect of onset, offset, duration, and event completeness on blink labeling, a specialized interpretation step was employed to establish a consistent mapping from segmented EOG events to communication symbols [12], [18].

Boundaries for making decisions have been calculated using the independent calibration data set that includes recordings of EOG activity for 25 subjects during the execution of voluntary single and double blink activities. The definition of the time of the blink, d_i, according to the boundaries given Eq.(5), was used together with two other temporal measures for the analysis of double blinks. The inter-blink time, g_i, is defined in Eq.(6) [18], while the total temporal measure,

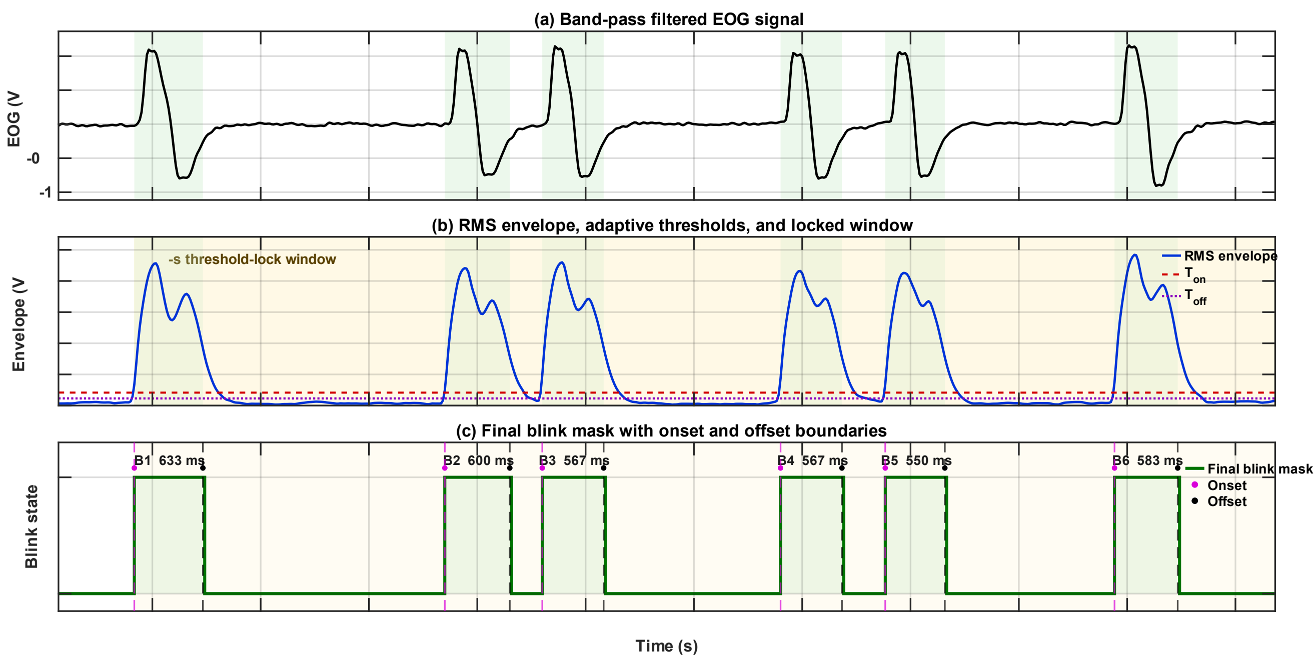

Fig. 2 Threshold-locked EOG blink extraction: (a) band-pass filtered EOG signal, (b) RMS envelope with adaptive onset/offset thresholds and a 20-second threshold-lock window, and (c) final state-based blink mask with onset and offset boundaries.

Manuscript received 13 May 2026; Revised 20 July 2026; Accepted 30 July 2026; Available online 10 August 2026
Digital Object Identifier (**DOI**): https://doi.org/10.35882/jeeemi.v8i4.1848

Δ_i^D, that represents a potential double blink is defined in Eq.(7) [18].

$$g_i = t_{on}^{(i+1)} - t_{off}^{(i)} \tag{6}$$

$$\Delta_i^D = t_{off}^{(i+1)} - t_{on}^{(i)} \tag{7}$$

where g_i refers to the temporal measure between two successive blink candidates, while Δ_i^D represents the total temporal measure of the potential double blink. The calibrated temporal boundaries for d_i, g_i, and Δ_i^D, along with the waveform-consistency parameters are shown in Table 1. This calibration phase eliminates arbitrary threshold selection and aligns the decision rules with the observed voluntary blinking behavior among participants. Temporal criteria alone may prove insufficient when a protracted single blink resembles a double-blink response or when two closely spaced blinks are largely conflated by residual blink tails. Consequently, the temporal decision was substantiated using autocorrelation-based waveform consistency and peak-based morphological validation. For each candidate segment $z_i(n)$ derived from the filtered EOG signal, the normalized autocorrelation was calculated as per Eq.(8) [32], [38]:

$$\rho_i(\ell) = \frac{\sum_{n=1}^{N_i-\ell}(z_i(n) - \bar{z}_i)(z_i(n+\ell) - \bar{z}_i)}{\sqrt{\sum_{n=1}^{N_i-\ell}(z_i(n) - \bar{z}_i)^2 \sum_{n=1}^{N_i-\ell}(z_i(n+\ell) - \bar{z}_i)^2}} \tag{8}$$

Let $z_i(n)$ be the i-th blink candidate that has been identified from the EOG signal, where N_i denotes the number of samples in the segment and $\bar{z}_i$ is the mean of $z_i(n)$. In this context, ℓ denotes the index of the lag in samples, which is equivalent to a time difference of ℓ/f_s seconds, where f_s is the sampling rate. The dimensionless normalized autocorrelation coefficient $\rho_i(\ell)$ compares the waveforms of the candidate segment and its delayed version at lag ℓ. This method was used to help interpret the temporal analysis by evaluating the self-consistency of the candidate blink segments before assigning them to the desired single or double blinks. Since autocorrelation measures the similarity between a signal segment and its delayed version, it was used here as a waveform-consistency descriptor for the segmented blink candidate [38]. The pattern-specific autocorrelation score, $A_q(i)$, as defined in this study as the maximum normalized autocorrelation value within the calibrated lag region of the corresponding blink pattern, is shown in Eq.(9):

$$A_q(i) = \max_{\ell/f_s \in \Omega_q} \rho_i(\ell), q \in \{S, D\} \tag{9}$$

where Ω_q represents the lag region that corresponds to the respective blinking pattern. In contrast, peak verification was done using the relative amplitude criteria rather than the absolute voltage criteria. The minimum permissible peak value was set from Eq.(10) as follows [39]:

$$H_{min,i} = r_H \max_n |z_i(n)| \tag{10}$$

where $z_i(n)$ is the filtered EOG signal segment related to the i-th blink candidate. Also, it is denoted by $\max_n |z_i(n)|$ the maximum absolute amplitude of this segment. The value of r_H= 0.25 is the calibrated height ratio given in Table 1. Thus, $H_{min,i}$ is not a constant voltage threshold but rather a variable one equal to 25% of the local segment's maximum amplitude. This ratio was selected experimentally using another calibration set to filter out small residual fluctuations while preserving legitimate low-amplitude peaks, especially for double blinks. Autocorrelation helps identify repeated blink patterns in restricted blink segments as mentioned in previous studies dealing with blink communication systems and blink-to-speech schemes [9], [31], [32], while peak verification adds an additional confirmation to the morphological structure of the filtered blink segment [40]. It demonstrates the examples of the S and D patterns along with their respective waveforms. The output results of the rule-based blink pattern interpretation phase, prior to decoding messages, are shown in Fig. 4 . This figure highlights how segmented EOG blink patterns are considered legitimate single- or double-blink patterns according to temporal criteria and verified by means of autocorrelation and peak verification. The use of autocorrelation ensures that the waveform is consistent in the lag range assumed, while peak verification ensures that the local peaks in the pattern match those of the intended blink pattern. As this example shows, the proposed method used timing and waveform information along with morphology to provide reliable labels S(0) and D(1), which were then used for message decoding. This interpretation algorithm used a double-first decision process, as illustrated in Fig. 3 . The algorithm will further analyze blink candidates and their corresponding onset time, offset time, duration, and gap between two consecutive blink candidates. The first decision in analyzing each of the blink candidates is to determine whether the current blink candidate and the following blink are part of a double blink sequence, depending on the temporal gates and evidence from autocorrelation and peak verification. When there is no acceptance of the double-candidate decision pathway, the current blink candidate is subjected to a test to determine if the blink is a single blink using the single blink duration gate and evidence. When two close blinks are observed as one merged blink candidate, the merged-double fallback pathway will be used, taking into account the duration of the segment, the structure of the peak inside the segment, and the autocorrelation evidence. Following acceptance of each single- or double-pattern, a brief post-acceptance guard interval was implemented to prevent reprocessing of residual blink tails or neighboring artifacts as independent candidates. The

Manuscript received 13 May 2026; Revised 20 July 2026; Accepted 30 July 2026; Available online 10 August 2026
Digital Object Identifier (**DOI**): https://doi.org/10.35882/jeeemi.v8i4.1848

final evidence-fusion rule was formulated in this study by combining three validated decision components: temporal gating; autocorrelation-range validation; and peak structure validation. This evidence is supported by previous research on blink characterization, correlation of blink communication, and threshold-based blink detection [18], [32], [39]. The conclusive combination evidence rule is expressed as in Eq. (11):

$$\widehat{P}_i = \begin{cases} D, T_D(i) = 1 \wedge (A_D(i) \in A_D \wedge PeakOK_D(i) = 1) \\ S, T_S(i) = 1 \wedge (A_S(i) \in A_S \wedge PeakOK_S(i) = 1) \\ U, Otherwise \end{cases} \quad (11)$$

In Eq.(11), let $\widehat{P}_i$ be the interpretation of the i-th candidate segment, which corresponds to the double blink, single-blink, and unknown patterns D, S, and U, respectively. The binary flags $T_D(i)$ and $T_S(i)$ are the temporal decision variables that indicate when the temporal calibration criteria for the double-blink and single-blink patterns are met. The variables $A_D(i)$ an $A_S(i)$ are the corresponding autocorrelation scores in the dimensionless form, and A_D and A_S stand for the accepted autocorrelation ranges provided in Table 1. The binary flags $PeakOK_D(i)$ and $PeakOK_S(i)$ show whether the detected peak structure confirms the pattern interpretation. The segments that did not meet the criteria were classified into U and excluded from the decoder to avoid any ambiguity in the Arabic message decoding. Therefore, the output from this phase of interpretation is not the message for communication

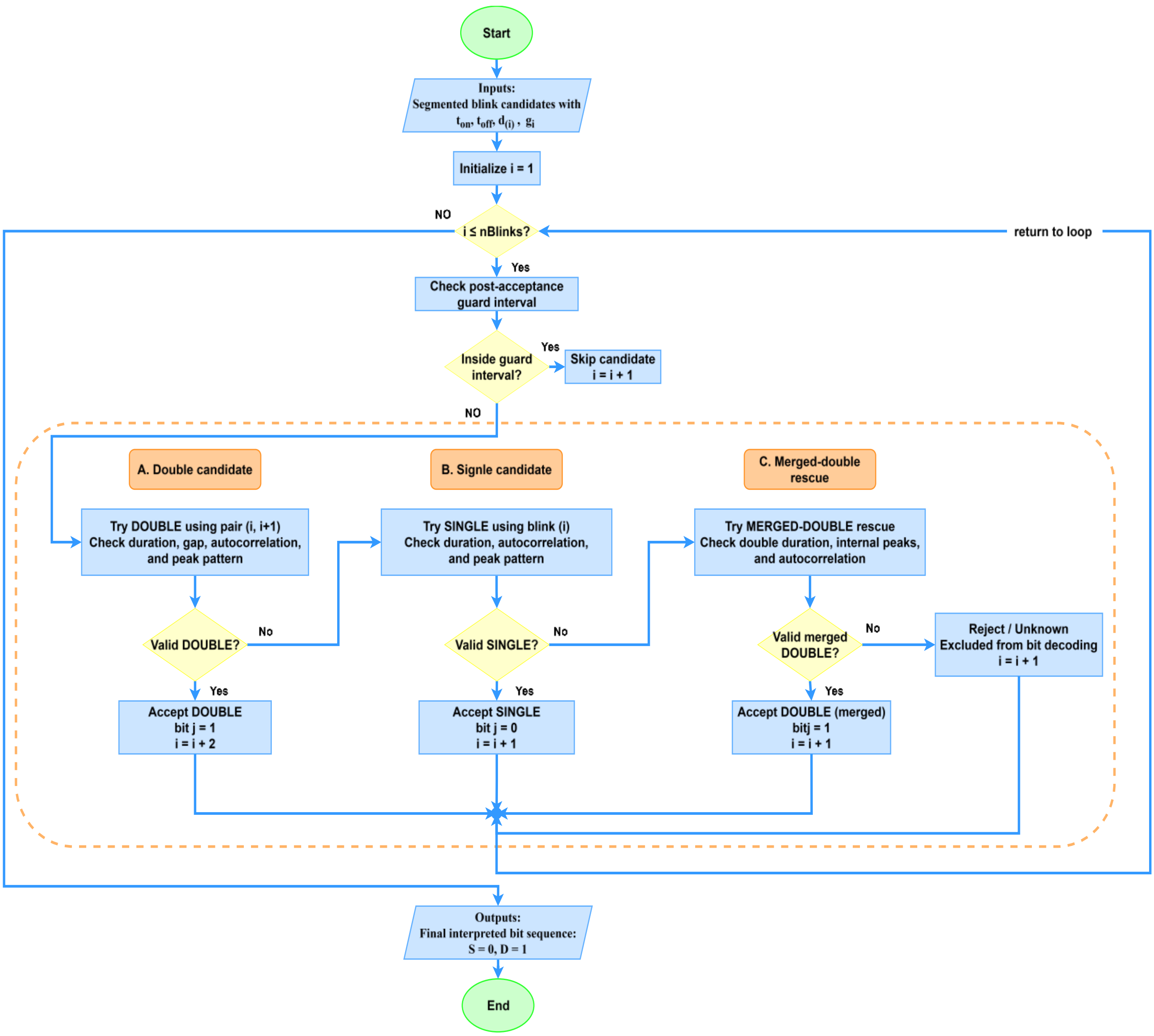

Fig. 3 Flowchart of the suggested algorithm for interpreting single and double blinks .This chart describes the decision-making process of the double-first option, the single-blink backup system, the double-merged checkup, the rejection of undefined event types, and the assignment of the S(0)/D(1) tag.

Manuscript received 13 May 2026; Revised 20 July 2026; Accepted 30 July 2026; Available online 10 August 2026
Digital Object Identifier (**DOI**): https://doi.org/10.35882/jeeemi.v8i4.1848

Journal of Electronics, Electromedical Engineering, and Medical Informatics
Homepage: jeeemi.org; Vol. 8, No. 4, October 2026, pp: 1331-1353 **e-ISSN: 2656-8632**

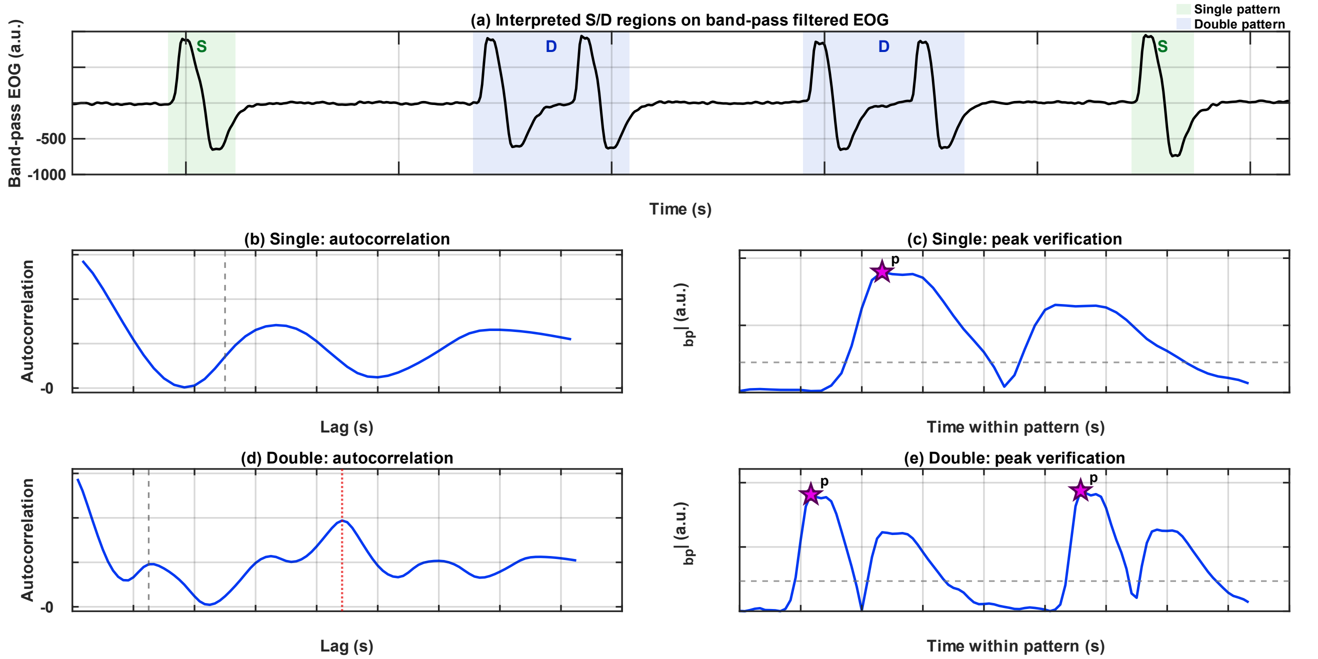

Fig. 4 Representative outputs of the proposed blink-pattern interpretation stage: (a) rule-based single/double blink interpretation on the band-pass filtered EOG signal, (b) autocorrelation validation for a single-blink candidate, (c) peak verification for a single-blink candidate, (d) autocorrelation validation for a double-blink candidate, and (e) peak verification for a double-blink candidate

but rather the verified set of blink label patterns. The labels with the codes S and D were sent to the decoding phase as binary values, while those coded as U or rejected are ignored to avoid distorting the four-bit Arabic message frame.

G. Rule-Based Decoding of Arabic Messages

The concluding phase of the proposed architecture transforms the verified temporal blink pattern labels into significant Arabic assistive messages using a rule-based message-level decoding technique. Electrooculography (EOG)-based assistive communication has been explored for individuals with significant motor impairments and communication restrictions associated with amyotrophic lateral sclerosis (ALS). Many current blink-based systems depend on sequential spelling, Morse-like coding, or code-by-code interaction, potentially increasing the number of necessary blinks and extending communication duration. Conversely, restricted vocabulary and blink-to-message methodologies might alleviate the interaction effort by correlating brief deliberate blink sequences directly to predetermined expressions. The suggested decoder will use a simple vocabulary-based design where a short combination of decoded voluntary blinks will represent a complete Arabic message in one go and not letter by letter. The operation of the decoder will be controlled under an open window signal quiet gate mechanism to avoid any spurious messages being produced. A word-level decoding window was initiated solely when the RMS envelope signaled an adequately quiet signal condition prior to the first acceptable blink pattern. This rule delineates a distinction between the resting state and the deliberate communication state, hence diminishing the likelihood of spontaneous blinks, residual activity, or transition artifacts being included in the message frame. Upon the activation of the word window, only temporally sequenced and verified blink-pattern labels were permitted for message formulation. The binary encoding for each approved pattern is as follows: a single-blink pattern is encoded as 0; while a double-blink pattern is encoded as 1. To construct a complete message frame for the proposed 16-message Arabic vocabulary, four validated blink-pattern labels are necessary. The four-bit message frame was defined in this study to represent the verified sequence of four blink-pattern labels, Eq.(12).

$$\boldsymbol{B} = [\boldsymbol{b_1 b_2 b_3 b_4}],\ \boldsymbol{b_i} \in \{\boldsymbol{0}, \boldsymbol{1}\}, \boldsymbol{i} = \boldsymbol{1}, \boldsymbol{2}, \boldsymbol{3}, \boldsymbol{4} \tag{12}$$

where B represents the sequence of four bits of the message frame, and $\boldsymbol{b_i}$ stands for the binary number corresponding to the blink pattern label i. This binary frame represented by Eq.(12) is later translated into a decimal number using Eq.(13) [41]:

$$\boldsymbol{d} = \sum_{\boldsymbol{i}=\boldsymbol{1}}^{\boldsymbol{4}} \boldsymbol{b_i 2^{4-i}}, \qquad \boldsymbol{d} \in \{\boldsymbol{0}\ , \boldsymbol{15}\} \tag{13}$$

The index d was then used to obtain the relevant Arabic auxiliary message from the suggested 16 message dictionary. The active word window closes with the acquisition of the initial complete four-bit frame. If the frame includes absent, invalid, or temporally inconsistent blink-pattern labels, the decoding attempt

Manuscript received 13 May 2026; Revised 20 July 2026; Accepted 30 July 2026; Available online 10 August 2026
Digital Object Identifier (**DOI**): https://doi.org/10.35882/jeeemi.v8i4.1848

Table 2 Four-Bit Arabic Assistive Message Dictionary for Rule-Based Blink Decoding

Binary frame	Decimal index	Arabic assistive message	English meaning
0000	0	نعم	Yes
0001	1	لا	No
0010	2	أعاني من صعوبة بالتنفس	I am having difficulty breathing
0011	3	أحتاج دوائي الان	I need my medication now
0100	4	أشعر بألم في الرأس	I have a headache
0101	5	أشعر بألم في المعدة	I have stomach pain
0110	6	أرغب في استخدام دورة المياه	I need to use the restroom
0111	7	أحتاج الى ماء	I need water
1000	8	أنا جائع او احتاج الى طعام	I am hungry or need food
1001	9	أرفع رأسي او سريري	Raise my head or bed
1010	10	أخفض رأسي او سريري	Lower my head or bed
1011	11	أدرني الى اليمين	Turn me to the right
1100	12	أدرني الى اليسار	Turn me to the left
1101	13	شغل او أطفى التلفاز من فضلك	Please turn the television on or off
1110	14	شغل او أطفى الانوار من فضلك	Please turn the lights on or off
1111	15	أفتح او أغلق النافذة	Open or close the window

is dismissed instead of being coerced into an output message. This conservative frame-validation technique is crucial, as a solitary bit-level error may lead to an erroneous final message. The decoding stage functions as a deterministic semantic mapping layer that converts confirmed EOG-derived blink patterns into concise Arabic communication signals, without incorporating an additional machine-learning classification phase. Table 2 shows the four-bit Arabic message lexicon used in the proposed phase of decoding. This message lexicon assigns an Arabic message to every binary frame based on functional communication considerations that include immediate answers, medical questions, basic requirements, location assistance, and comfort of the surroundings.

H. Algorithm for Proposed Pipeline

To provide more clarity about how the pipeline will work, an algorithm has been provided below. This is Algorithm 1, and it clearly states how RMS envelope generation, state machine-based blink detection, single- and double-blink interpretations, and, finally, message decoding of four-bit Arabic characters would be accomplished.

Algorithm Proposed vertical-EOG blink-to-message decoding pipeline.

(1) **Input:** Raw vertical-EOG signal x(n), timestamp vector t(n), sampling frequency fs, calibrated parameters in Table 1, and the Arabic message dictionary in Table 2.
(2) **Output:** Detected blink-event set E, four-bit frame B, and decoded Arabic message M or an incomplete/invalid-frame result.
(3) **Initialization:** Set E → ∅, P → ∅, B → [ ], state → QUIET, and lock → false, where P is the interpreted blink-pattern sequence.
(4) Remove the DC component and impulsive artifacts, apply the second-order 0.2–15 Hz Butterworth band-pass filter, and compute the RMS envelope e(n).
(5) Estimate the initial quiet-background statistics from the 5-s baseline and initialize Ton and Toff using Eq. (1) and Eq. (2).
(6) FOR each RMS-envelope sample e(n) DO.
(7) IF state = QUIET, lock = false, and the threshold-update interval has elapsed THEN update the quiet-background statistics and recalculate T_{on} and T_{off}.
(8) IF state = QUIET and the validated onset condition is satisfied THEN record the blink onset, lock T_{on} and T_{off} for the 20-s communication window, set lock → true, and set state → ACTIVE.
(9) ELSE IF state = ACTIVE THEN update the event peak and adaptive ending level using Eq.(4); when the event-ending condition is satisfied, record the blink offset and duration using Eq. (5), append the event to E, and set state → REFRACTORY.
(10) ELSE IF state = REFRACTORY and the refractory interval has elapsed THEN set state → QUIET.
(11) End IF.
(12) IF the 20-s communication window has expired THEN set lock → false.
(13) End FOR
(14) Set i → 1
(15) WHILE i ≤ |E| DO
(16) IF events E_i and E_{i+1} satisfy the calibrated double-blink criteria THEN append D to P and set i → i + 2.
(17) ELSE IF event E_i satisfies the calibrated single-blink criteria, THEN append S to P and set i → i + 1.

Manuscript received 13 May 2026; Revised 20 July 2026; Accepted 30 July 2026; Available online 10 August 2026
Digital Object Identifier (**DOI**): https://doi.org/10.35882/jeeemi.v8i4.1848

(18) ELSE IF event E_i satisfies the calibrated merged-double criteria, THEN append D to P and set i → i + 1.
(19) ELSE append U to P and set i → i + 1.
(20) END IF
(21) Apply the post-acceptance guard interval after each accepted S or D pattern.
(22) END WHILE.
(23) Open the word window only when the pre-frame raw-envelope quiet condition is satisfied.
(24) Collect four temporally ordered pattern labels within the active word window.
(25) IF four valid S/D pattern labels are obtained, THEN map S → 0 and D → 1, and form B = [b1, b2, b3, b4] using Eq. (12).
(26) Calculate the decimal index using Eq. (13) and retrieve the corresponding Arabic assistive message M from Table 2.
(27) ELSE set M → "Incomplete/invalid frame" when any pattern position is unknown, missing, or temporally invalid.
(28) END IF
(29) RETURN E, B, and M.

I. Performance Evaluation Metrics

The planned EOG-based pipeline was assessed utilizing 4,000 word-level recordings. The assessment was performed at three sequential stages: blink-event identification, rule-based interpretation of blink patterns, and ultimate decoding of the Arabic message. The projected blink segments were compared to the protocol-derived ground-truth blink windows at the detection level. At the blink-pattern interpretation level, the anticipated single- and double-blink interpretation were juxtaposed with the respective target pattern labels. At the ultimate decoding stage, the anticipated four-bit blink frame was juxtaposed with the intended Arabic helpful message. In blink-event detection, true positives (TP), false positives (FP), and false negatives (FN) were utilized to calculate precision, recall, and F1-score as follows in Eq.(14), Eq.(15), Eq.(16) [42]:

$$\boldsymbol{Precision} = \frac{\boldsymbol{TP}}{\boldsymbol{TP}+\boldsymbol{FP}} \tag{14}$$

$$\boldsymbol{Recall} = \frac{\boldsymbol{TP}}{\boldsymbol{TP}+\boldsymbol{FN}} \tag{15}$$

$$\boldsymbol{F1} = \frac{\boldsymbol{2}\times\boldsymbol{Precision}\times\boldsymbol{Recall}}{\boldsymbol{Precision}+\boldsymbol{Recall}} \tag{16}$$

The temporal localization of the identified blink events was assessed by calculating the absolute midpoint timing inaccuracy between each matched predicted blink window and its matching ground-truth blink window, as shown in Eq.(17) [43]:

$$\boldsymbol{e_i} = |\boldsymbol{t^{pred}_{mid,i}} - \boldsymbol{t^{GT}_{mid,i}}| \tag{17}$$

Let $t^{Pred}_{mid,i}$ and $t^{GT}_{mid,i}$ be the midway times of the predicted and ground truth blink intervals, respectively.

The mean absolute midpoint error (MAE_{mid}) was subsequently calculated as Eq.(18) [43]:

$$\boldsymbol{MAE_{mid}} = \frac{\boldsymbol{1}}{\boldsymbol{N_m}}\sum_{\boldsymbol{i=1}}^{\boldsymbol{N_m}}\boldsymbol{e_i} \tag{18}$$

N_m denotes the quantity of matching blink occurrences. For interpreting blink patterns, pattern-level accuracy, balanced accuracy, and macro-F1 scores were calculated for both single- and double-blink target patterns, as shown in Eq.(19), Eq.(20), Eq.(21), Eq.(22) [42]:

$$\boldsymbol{Accuracy} = \frac{\boldsymbol{N_{correct}}}{\boldsymbol{N_{total}}} \tag{19}$$

$$\boldsymbol{Balanced\ Accuracy} = \frac{\boldsymbol{Recall_S}+\boldsymbol{Recall_D}}{\boldsymbol{2}} \tag{20}$$

$$\boldsymbol{MacroF1} = \frac{\boldsymbol{F1_S}+\boldsymbol{F1_D}}{\boldsymbol{2}} \tag{21}$$

$$\boldsymbol{UnknownRate} = \frac{\boldsymbol{N_{unknown}}}{\boldsymbol{N_{total}}} \tag{22}$$

where $Recall_S$ and $Recall_D$ denote the class-specific recall values for the single- and double-blink patterns, respectively, while $F1_S$ and $F1_D$ denote their corresponding class-specific F1-scores. $N_{correct}$, $N_{unknown}$, and N_{total} denote the numbers of correctly interpreted, unknown, and total evaluated pattern slots, respectively. At the ultimate message-decoding stage, the decode-valid rate and final Arabic message accuracy were computed as follows in Eq.(23), Eq.(24) [42]:

$$\boldsymbol{DecodeValidRate} = \frac{\boldsymbol{N_{valid}}}{\boldsymbol{N_{attempts}}} \tag{23}$$

$$\boldsymbol{Message\ Accuracy} = \frac{\boldsymbol{N_{correct\ message}}}{\boldsymbol{N_{attempts}}} \tag{24}$$

where $N_{attempts}$, N_{valid}, and $N_{correct\ message}$ denote the total message attempts, valid four-bit outputs, and correctly decoded Arabic messages, respectively. A frame was considered valid only when all four pattern positions produced accepted binary labels. A decoded message was considered correct only when the entire predicted four-bit frame exactly matched the target frame and consequently corresponded to the intended Arabic assistive message.

To assess the stability of the proposed pipeline across subjects and identify any possible inter-subject variance hidden within aggregate performance measures, the analysis was performed on an individual subject basis, with each of the 25 subjects performing 160 word-level trials. To measure different functional components of the proposed pipeline, three performance metrics were selected corresponding to the pipeline's consecutive steps: F1-score for blink-event detection, accuracy for blink-pattern interpretation, and exact accuracy for Arabic message reproduction. Separating the examination of the

Manuscript received 13 May 2026; Revised 20 July 2026; Accepted 30 July 2026; Available online 10 August 2026
Digital Object Identifier (**DOI**): https://doi.org/10.35882/jeeemi.v8i4.1848

performance metrics makes it possible to pinpoint inter-subject variance in event extraction, pattern interpretation, or message decoding. Such subject-level analysis is especially relevant for the EOG-based blink interaction, since the timing and morphology of the blink may differ from one subject to another and even across repeated trials within the same subject [42]. For each performance metric m, the subject-level mean, sample standard deviation, 95% confidence interval, and min-max range were calculated according to Eq.(25), Eq.(26), Eq.(27) [42].

$$\bar{P}_m = \frac{1}{N_s}\sum_{s=1}^{N_s} P_{m,s} \tag{25}$$

$$SD_m = \sqrt{\frac{1}{N_s - 1}\sum_{s=1}^{N_s}(P_{m,s} - \bar{P}_m)^2} \tag{26}$$

$$95\%CI_m = \bar{P}_m \pm t_{0.975,N_s-1}\frac{SD_m}{\sqrt{N_s}} \tag{27}$$

where m refers to the performance metric being analyzed, s refers to the subject index, $P_{m,s}$ refers to the value of the metric m for subject s, N_s refers to the total number of subjects analyzed, $\bar{P}$ refers to the mean value of metric m, SD_m refers to the standard deviation of metric m, and $t_{0.975,N_s-1}$ refers to the critical value of the t-distribution. In the present evaluation, Ns=25. The observed minimum–maximum range was obtained directly from the smallest and largest participant-specific values.

III. Results

A. Overall Pipeline Performance

The overall quantitative performance of the proposed pipeline at the blink-event detection, blink-pattern interpretation, and message-decoding levels is summarized in Table 3. For the first level, the blink-event detector reached 97.37% precision, 94.06% recall, and 95.69% F1-score with a mean absolute midpoint error of 206.96 ms, demonstrating successful extraction and localization of voluntary blink events. The second level showed that the detected single and double-blink patterns achieved 98.10% accuracy and 98.30% macro-F1, and 0.40% of pattern slots were tagged as unknown by the system. Finally, the third level showed that 98.55% of trials yielded four-bit frames, resulting in an exact Arabic message accuracy of 92.98% and a macro-F1 of 93.67% for the messages. It should be noted that the discrepancy between pattern and message results is caused by the cumulative nature of decoding, in which one incorrect bit can change the entire decoded message.

B. Subject-level Performance

Following the aggregate results presented in Table 3, participant-level performance was analyzed across the three pipeline stages to examine inter-subject variability. As summarized in Table 4, the degree of variability differed among blink-event detection, blink-pattern interpretation, and message decoding. The interpretation of the blink pattern proved to be the most consistent stage in the cohort, showing 98.1±1.4% accuracy with a narrow observed range of 95.00–99.84%. The minimum accuracy was achieved for S25, while S4, S7, and S13 had the highest value. This small dispersion suggests that, after successful extraction of blink events, the rules for temporal and morphological interpretation proved quite consistent despite differences in individual signals. Event extraction showed somewhat higher variability between participants, ranging from 88.84% for S24 to 98.97% for S4, with the cohort mean of 95.5±2.4%.

Table 3 Comprehensive quantitative assessment of the proposed EOG-based detection-to-message pipeline.

Evaluation level	Metric	Result
Blink-event Detection	Precision	97.37%
	Recall	94.06%
	F1-score	95.69%
	Mean absolute midpoint error (MAE)	206.96 ms
Blink-pattern Interpretation	Accuracy	98.10%
	Macro-F1	98.30%
	Balanced Accuracy	98.10%
	Unknown Rate	0.40%
Arabic message decoding	Decode-valid rate	98.55%
	Message Accuracy	92.98%
	Macro-F1	93.67%

The greatest inter-participant variability was observed at the last decoding stage, with message accuracy averaging 92.9±5.5%, ranging from 80.00% for S25 to 99.38% for S4, S7, and S13. The broader dispersion here does not indicate the individual instability of deterministic message mapping; instead, it demonstrates the cumulative requirement for correct interpretation of all four pattern positions to generate the exact message. In this way, any residual error or unknown output at one position propagates to the message decoding stage, altering or invalidating the message itself. The fact that the lowest detection F1-score corresponded to S24, while the lowest interpretation and message accuracy corresponded to S25, suggests that participant-specific problems are not consistently observed across pipeline stages. Generally speaking, Table 4 shows that pattern interpretation proves quite reliable across all evaluated participants, whereas message-level performance

Manuscript received 13 May 2026; Revised 20 July 2026; Accepted 30 July 2026; Available online 10 August 2026
Digital Object Identifier (**DOI**): https://doi.org/10.35882/jeeemi.v8i4.1848

Journal of Electronics, Electromedical Engineering, and Medical Informatics
Homepage: jeeemi.org; Vol. 8, No. 4, October 2026, pp: 1331-1353 e-ISSN: 2656-8632

becomes more sensitive to the accumulation of earlier-stage errors.

Table 4 Performance Analysis of Subjects over the 25 Evaluation Subjects.

Subject	Detection F1 %	Pattern accuracy %	Word accuracy %
S1	94.15	96.88	88.75
S2	95.59	98.75	95.00
S3	95.40	97.34	89.38
S4	98.97	99.84	99.38
S5	96.42	98.91	95.63
S6	95.16	97.34	90.63
S7	98.69	99.84	99.38
S8	95.90	98.44	95.63
S9	97.72	99.38	98.13
S10	95.91	99.06	96.25
S11	97.68	98.13	94.38
S12	98.10	98.59	95.63
S13	98.53	99.84	99.38
S14	90.22	98.13	92.50
S15	94.17	98.13	93.13
S16	93.39	98.44	94.38
S17	96.34	99.06	96.25
S18	95.96	97.81	91.25
S19	94.70	98.75	95.00
S20	96.88	99.22	97.50
S21	95.95	95.16	81.25
S22	97.80	98.91	96.88
S23	92.58	95.78	83.75
S24	88.84	95.78	85.00
S25	94.48	95.00	80.00
$\bar{P}_m \pm SD_m$	95.5 ± 2.4	98.1 ± 1.4	92.9 ± 5.5
$95\%CI_m$	94.5 – 96.6	97.5 – 98.6	90.6 – 95.2
Min – Max	88.8 – 98.9	95.0 – 99 .8	80.0 – 99.3

C. Interpretation of Single/Double Blink Patterns

The second stage of pattern interpretation accuracy evaluation assessed the reliability of rule-based pattern interpretation in assigning detected and temporally segmented blink events from the previous stage to either single- or double-blink patterns. While Table 3 reflects the aggregate pattern-level performance, the row-normalized matrix shown in Fig. 5 illustrates the distribution of pattern-interpretation results for each ground-truth class. This allows independent evaluation of the relative pattern-level performance of the two target patterns, the direction of pattern-interpretation errors, and the distribution of unknown pattern-interpretation results.

As shown in Fig. 5 , of the 8,000 ground-truth single-blink slots, 7,907 (98.8%) were successfully interpreted as such patterns, while 7,789 of 8,000 double-blink slots (97.4%) were classified. The majority of pattern interpretation errors related to double-blink patterns were misinterpretated as single blinks (193 instances, 2.4%), while single-blink patterns were misinterpreted as double-blinks only 47 times (0.6%). Detailed analysis of the corresponding EOG recordings and the pipeline's intermediate stages revealed that misinterpretation of the double-blink pattern primarily resulted from insufficient temporal or morphological separation between the two blinks. In some cases, the interval between the two blinks fell below the calibration threshold for temporal separation, resulting in incomplete response separation and the merging of the two into a single temporal candidate. Also, in some recordings, the second response of the double-blink pattern had low amplitude; therefore, the peak verification and autocorrelation conditions necessary for the double-blink pattern were not satisfied. This result is consistent with prior blink studies based on video-verified blinks, where it was observed that close-in-time or low-amplitude blink pairs are not always separated [44]. However, detailed analysis of relatively rare cases of misinterpreting single blinks as double blinks showed that some slowly performed or long-lasting blinks exhibited a multiphasic morphology. A decrease followed by an increase in the RMS envelope, or the appearance of two well-separated peaks within a single blink, caused it to be segmented into two separate candidates and to meet the temporal or morphological criteria necessary for being considered a double blink. The occurrence of these misinterpretations varied across participants and runs, reflecting both inter-subject and intra-subject variability in the temporal execution and morphology of voluntary blinks [44]. Within-session variability might also be caused by repeated task execution, since blink duration and blink rate have been shown to vary depending on time on task and fatigue; however, fatigue level was not

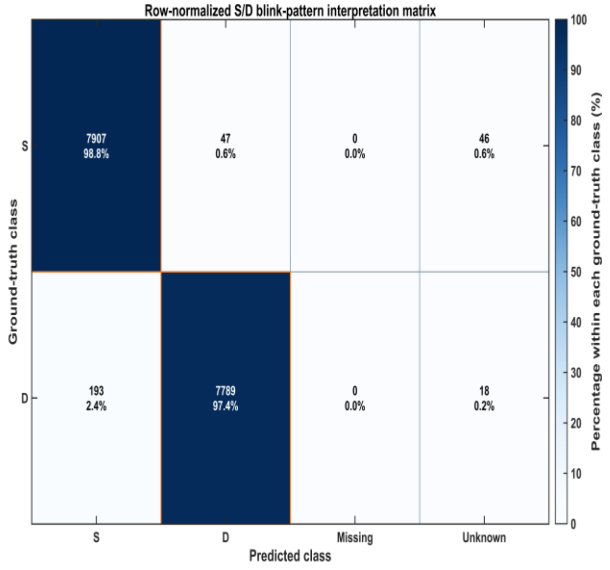

Fig. 5 Row-normalized single/double blink-pattern interpretation matrix.

Manuscript received 13 May 2026; Revised 20 July 2026; Accepted 30 July 2026; Available online 10 August 2026
Digital Object Identifier (**DOI**): https://doi.org/10.35882/jeeemi.v8i4.1848

evaluated separately in the current experiment and cannot be considered as the reason for misinterpretation [45]. Unknown outputs were limited to 46 single-blink pattern slots (0.6%) and 18 double-blink pattern slots (0.2%), yielding an unknown rate of 0.40% as shown in Table 3, and there were no missing pattern outputs in any class.

D. Message-Level Per-Class and Confusion Matrix Analysis

Finally, the third stage examined the propagation of the interpretation errors through the deterministic four-bit mapping process and their effect on message decoding. The analysis of the entire dataset shows that in 98.55% of cases, valid four-bit frames were produced. Using the exact-frame criterion, the message decoding accuracy reaches 92.98%, while the macro-F1 score is 93.67%. The row-normalized per-class metrics in Fig. 6, and the detailed per-class metrics in Table 5 suggest that the performance on messages was fairly balanced across all 16 communication classes with F1-scores ranging from 90.6% to 96.1%. However, the error distribution was unbalanced. The class W12 achieved the best overall performance, with an F1 score of 96.1%, while the worst performance was achieved by class W05, with the lowest precision of 89.1% and an F1 score of 90.6%. At the same time, classes W11 and W13 had the lowest recall, at 89.2%, indicating that a larger share of intended four-bit frames was transferred to other decoded messages or deemed invalid.

Looking at the structure of the confusion matrix in Fig. 6, it becomes clear that the differences in class-level performance follow a certain bit transition pattern rather than a message substitution. The most common error type was the substitution of W13 for W05, which occurred in 21 trials (8.4%), followed by W14→W06 and W15→W07 (17 trials each, 6.8%), and W16→W08 (12 trials, 4.8%). In all of those cases, the final three bits were preserved while the first bit changed from 1 to 0. As those numbers correspond to the double- and single-blink patterns, it is evident that a double blink in the first pattern position was mistakenly recognized as

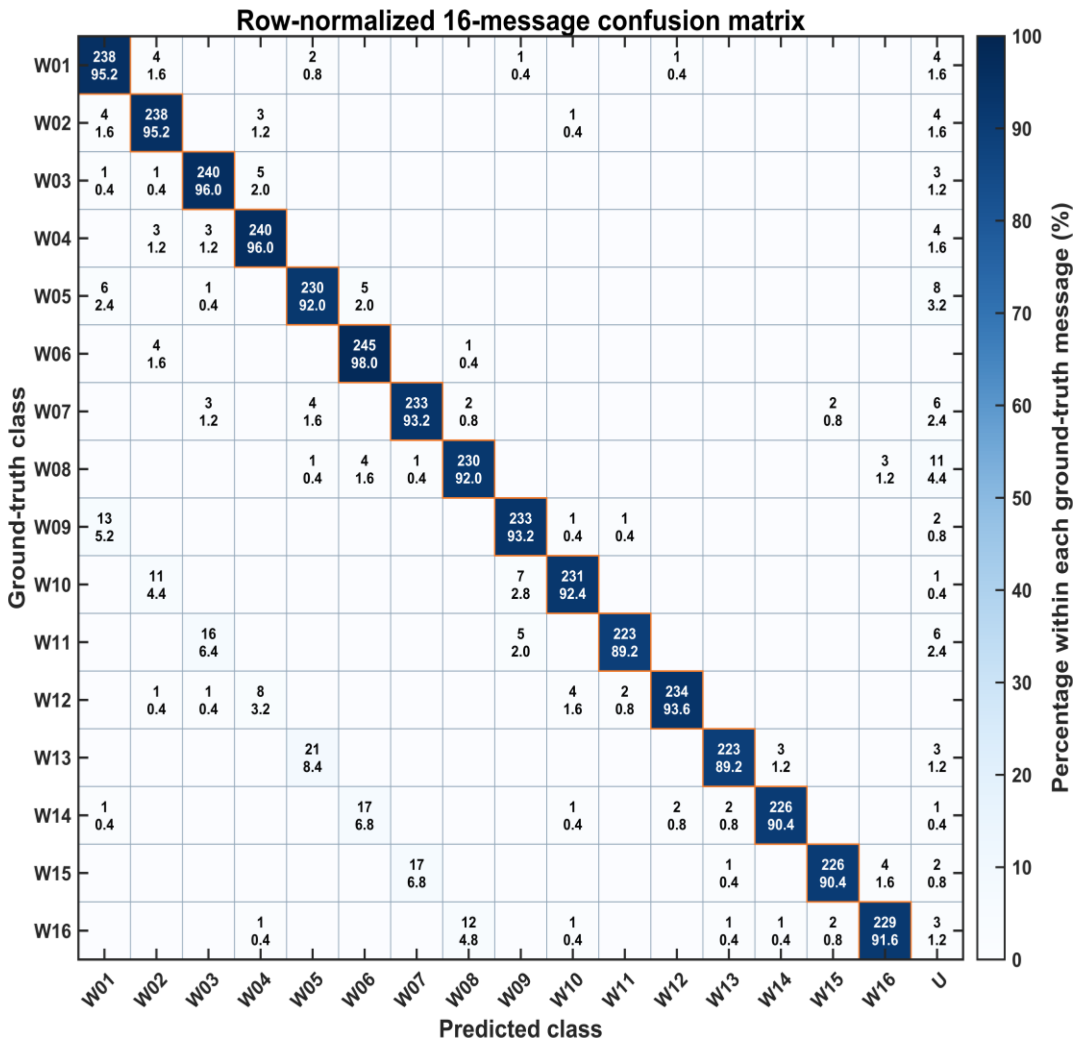

Fig. 6 Row-normalized message-level confusion matrix for the 16 Arabic assistive messages.

Manuscript received 13 May 2026; Revised 20 July 2026; Accepted 30 July 2026; Available online 10 August 2026
Digital Object Identifier (**DOI**): https://doi.org/10.35882/jeeemi.v8i4.1848

Table 5 Per-class precision, recall, and F1-score for the 16 Arabic assistive messages.

Message index	Bit frame	Precision (%)	Recall (%)	F1-score (%)
W01	0000	90.5%	95.2%	92.8%
W02	0001	90.8%	95.2%	93.0%
W03	0010	90.9%	96.0%	93.4%
W04	0011	93.4%	96.0%	94.7%
W05	0100	89.1%	92.0%	90.6%
W06	0101	90.4%	98.0%	94.0%
W07	0110	92.8%	93.2%	93.0%
W08	0111	93.9%	92.0%	92.9%
W09	1000	94.7%	93.2%	94.0%
W10	1001	96.7%	92.4%	94.5%
W11	1010	98.7%	89.2%	93.7%
W12	1011	98.7%	93.6%	96.1%
W13	1100	98.2%	89.2%	93.5%
W14	1101	98.3%	90.4%	94.2%
W15	1110	98.3%	90.4%	94.2%
W16	1111	97.0%	91.6%	94.2%

a single blink. That created a frame that was still a valid four-bit code, and mapped to a message of some other class. This explains why some classes have high precision but low recall, and it also clarifies why W05 receives additional predictions transferred from W13, resulting in the lowest precision among all classes. Another type of error is evident in the U category in Fig. 6, with class-specific results shown in the recall and F1-score in Table 5. In this case, there are 58 trials (1.45%) where at least one position of the blink pattern is identified as unknown or in which no complete four-bit frame could be generated. The decoder did not classify these uncertain frames under any of the preset Arabic messages and withheld the message output, resulting in an overall decode validity rate of 98.55%. The most frequent rejections occur in W08 (4.4%) and W05 (3.2%), resulting in lower recall values for these classes in Table 5. The rejected frames differ in their performance impacts from off-diagonal message replacements, while rejection lowers the source class recall when no alternative message is predicted, replacement simultaneously affects the intended class recall and the erroneous class precision. Therefore, Fig. 6 and Table 5 show two kinds of downstream error propagation of upstream pattern-interpretation mistakes: a bit replacement, which turns the intended frame into a different message code, and a frame rejection as a result of one or several uncertain pattern positions.

IV. Discussion

The multi-level experiment shows that the developed pipeline for vertical-EOG-based assistive message composition has demonstrated stable performance throughout all levels necessary for such a task. The blink detection achieved an F1-score of 95.69%, yielding segmented events for further analysis. Then, the interpretation level using the rule-based approach achieved a macro-F1 of 98.30%, indicating that the tuned temporal and morphological rules have successfully addressed the problem of classifying single- and double-blink patterns. Finally, the Arabic message decoder achieved 92.98% accuracy and a macro-F1 of 93.67%. The relatively poor results on this step are due to the fact that four-position decoding is required for a message to be considered correct, while the deterministic nature of the message dictionary does not imply any ambiguity. The message is correct if all of its constituent patterns are correct, but the substitution of one pattern for another changes the whole message.

Event-level performance can be ascribed to the stabilization of both the EOG representation and detector state. The transformation of the band-pass signal to an RMS envelope resulted in a smooth, positive-energy trace with less energy dependence on signal polarity and created a robust foundation for segmentation by time. Hysteresis thresholds adapted only from the quiet-background signal allowed the detector to adjust to gradual changes in the baseline and amplitude of the signal without introducing any activity associated with blinking into the background model, and locking of the thresholds guaranteed the constancy of decision thresholds in the active message window. This approach is especially important for voluntary blinking, since amplitude, duration, completeness, and timing of the signal may differ between subjects and trials [18]. In addition, rule-based design ensures transparency of the signal processing chain through independent analysis of envelope construction, threshold crossing, event termination, and refractoriness control. However, fixed temporal and morphological requirements are still susceptible to abnormal behavior close to the decision boundary, which warrants further analysis of pattern- and message-level mistakes and development of an adaptive approach [21].

As for blink-pattern interpretation, the developed scheme achieved 98.10% accuracy and a 98.30% macro-F1 measure, with 98.8% and 97.4% correctness rates for single and double blink patterns, respectively. It is necessary to emphasize the slightly lower quality in the case of double blinks, which is associated with the more complex time and morphological structure of such responses, since the correct double-blink identification requires successful response detection along with appropriate individual duration, time interval between blinks, total pattern duration, presence of autocorrelation evidence, and the structure of peaks. In the case of a rapid succession of two blinks, the RMS

Manuscript received 13 May 2026; Revised 20 July 2026; Accepted 30 July 2026; Available online 10 August 2026
Digital Object Identifier (**DOI**): https://doi.org/10.35882/jeeemi.v8i4.1848

envelope may not have enough time to return to baseline, resulting in a single temporal candidate. In addition, the poor quality of the second response and insufficient evidence from two-peak and autocorrelation analyses can distort the interpretation of double blinks, leading to their incorrect classification as single blinks. On the other hand, the infrequent error of transitioning from single blinks to double ones was related to slow and long single blinks generating a multiphasic RMS envelope or two separate internal peaks combined with overlapping eye movements or nearby fluctuations of waveforms, thus making them similar to a double-blink response structure. Both types of reciprocal errors are typical due to the natural inter- and intra-subject variability in the voluntary execution of blinks and do not indicate a significant interpretative bias towards either pattern [44]. In ambiguous cases or cases when the candidate had an inappropriate temporal structure, they were classified as unknown, limiting the unknown rate to 0.40%.

However, the message-level confusion pattern was not uniformly distributed among the sixteen classes. Specifically, as shown in Fig. 6, some pronounced off-diagonal transitions occur between messages that have the last three bits identical but differ in the leading bit, namely W13 (1100)→W05 (0100), W14 (1101)→W06 (0101), W15 (1110)→W07 (0110), and W16 (1111)→W08 (0111). Here, the arrow denotes the direction of a message-decoding error from the intended message on the left to the decoded message on the right. For example, W13 (1100) → W05 (0100) means that the intended message W13 was incorrectly decoded as W05. The occurrence of those transitions can be attributed to a case in which the opening double-blink pattern is encoded by a single blink. A possible reason for this phenomenon is the timing of the first intentional response: the opening pattern occurs after the quiet baseline and the first cue, requiring a transition from relaxation to active blinking. In view of individual differences in cue perception, motor preparation, and response execution time, the first pattern can start later than the time allocated in the pattern's time window. If the first pattern is to be executed as a double blink, it can be done very quickly, reducing the inter-blink interval. In the case of RMS-envelope smoothing and state-based termination of events, a reduction in the envelope difference between the two responses can lead to their interpretation as a single candidate; if the internal peak and autocorrelation measures are also too low, the first bit would be encoded as 0 instead of 1. It should be considered an error associated with protocol-induced timing effects, not due to any intrinsic deficiencies of the first bit. Since all four-bit combinations are valid codes for Arabic messages, the resulting substitution is a correct code and is thus mapped to a different message. However, an unknown pattern at that position renders the frame incomplete and prevents decoding. The small F1 range of 90.6%–96.1% suggests that message errors were mainly caused by temporal decoding errors rather than message mapping ambiguity [10].

The mean absolute midpoint error of 206.96 ms should be interpreted as a temporal mismatch between the time of blink detection and the protocol-defined interval for that event, rather than as an indication of processing latency for the decoded message. Since this measure is based on the absolute midpoint difference, it does not show whether the detected event was occurring consistently earlier or later than the reference event. The noted deviation could be due to natural inter-trial variations in the timing of the voluntary blink response to the protocol trigger, as well as to RMS-envelope smoothing and event boundary detection. The voluntary blink response can be timed to occur after receiving the external trigger, yet the onset and peak of this event do not coincide across repeated trials, especially when there is no feedback on timing. The temporal variation in a real-time system would require sufficient tolerance, but the latency from executing the blink to the message being displayed needs to be assessed independently. The accuracy rates for the exact message with assistive devices were 92.98%, which means that approximately 93 out of 100 attempts showed the intended Arabic message in the offline test environment. The other 7 attempts consist of rejected trials and acceptable but unintended message codes, the latter being more important since they result in the display of a meaningful message that is not the user's desired request. Thus, the achieved performance demonstrates the technical capability of structured message communication in Arabic, while critical information messages will need to be verified with the intended users before clinical deployment.

Table 6. outlines an important trade-off between communication flexibility, interaction burden, and the state of evidence supporting them. Flexible communication is achievable through character- and Morse-like blinking schemes; however, their varying-length sequences cause repetition of blink generation, increase the duration of communication time slots, and increase the risk of accumulated coding mistakes [31], [47]. In contrast, predefined-message schemes reduce sequencing by mapping short, fixed code words to full messages; however, the message space is limited by the vocabulary size [7], [32]. The third trade-off concerns the acquisition modality: Camera-based interfaces eliminate electrode placement and provide both visual and synthesized speech output, yet require accurate eye tracking, a steady head position, and optimal image-processing conditions [7], whereas EOG-based schemes collect ocular activity directly but demand steady electrode–skin contact. Hence,

Manuscript received 13 May 2026; Revised 20 July 2026; Accepted 30 July 2026; Available online 10 August 2026
Digital Object Identifier (**DOI**): https://doi.org/10.35882/jeeemi.v8i4.1848

accuracy rates cannot be compared directly because they refer to different goals (eye-tracking accuracy, character selection, word building, and exact decoding of complete messages) [7], [31], [32]. Similarly, real-time operation does not imply fast communication when several selections or responses are encoded in a message and are needed for final message composition [7], [46]. From clinical studies, it is clear that results obtained in healthy subjects do not generalize to ALS patients, who may have lower communication accuracy and speed [47]. This list of trade-offs is supplemented in this research paper by direct vertical EOG acquisition, interpretable blink-pattern analysis, rejection of uncertain frames, and exact decoding of 16 complete Arabic assistive messages.

On the safety side, the current decoder provides a first conservative level of protection by dropping any unknown, incomplete, or temporally invalid frame without issuing a message. The current drop scheme, however, does not prevent all cases where a single-bit change yields another valid message. For a potential real-time implementation, each decoded message must be displayed in Arabic characters and/or spoken aloud before transmission. A separate window for confirmation of the decoded message will allow a

Table 6. A Quantitative Comparison with Recent Assistive Communication Systems Based on Eye and Blink Interactions

Study	Participants / population	Modality / mode	Output and coding burden	Performance / reported communication time
Verbaarschot et al., 2021 [47]	20 healthy participants and 10 users with ALS	Visual cVEP–EEG BCI; online	Full-keyboard spelling and binary Yes/No selection; repeated visual selections are required for text construction	Spelling accuracy: 79% in ALS, 88% in older healthy users, and 94% in younger healthy users; Yes/No accuracy ≈90%; ALS users achieved ≈10 characters/min
Ikizler et al., 2023 [32]	20 healthy participants, aged 20–55; no clinical users	Single-channel EEG/FP1 using NeuroSky; recorded-data evaluation	16 predefined expressions encoded by four single/double-blink positions; equivalent to 4–8 physical blinks per expression	Overall system accuracy: 98.75%; approximately 12 s/expression, corresponding to about five expressions/min
Ekim et al., 2023 [31]	10 healthy participants, aged 20–55; no clinical users	Single-channel EEG/FP1 using NeuroSky; offline evaluation	20 Turkish words constructed letter by letter using variable-length single, double, and triple blinks, with triple-blink letter/word delimiters	Word accuracy ranged from 94.0% to 99.5%; approximately 5–6 letters/min in healthy users
Ezzat et al., 2023 [7]	10 healthy participants, aged 21–79; no clinical users	Mobile camera and computer vision; real-time 64	predefined phrases, each represented by three states selected from left, right, up, and blink; one week of initial training	Participant-level phrase performance ranged from 10/27 to 27/27 tested phrases; 15–25 s/phrase on the mobile system and ≈3 s in the desktop test
Ding et al., 2024 [46]	One healthy 24-year-old male; personalized evaluation	No patients tested Dual-channel EOG with DC-CNN; real-time 40-key virtual keyboard	directional eye movements control the cursor and a double blink confirms each character	Real-time classification: 98.5%; character accuracy: 98.2% at 5.8 s/character; paragraph accuracy: 97.6% at 7.6 s/character
Proposed study	25 healthy participants; no clinical users	Direct vertical EOG using BioAmp and Arduino	offline 16 complete Arabic assistive messages encoded by four fixed single/double-blink positions4–8 physical blinks per complete message	Detection F1: 95.69%; pattern macro-F1: 98.30%; exact-message accuracy: 92.98%; end-to-end communication time was not measured

Manuscript received 13 May 2026; Revised 20 July 2026; Accepted 30 July 2026; Available online 10 August 2026
Digital Object Identifier (**DOI**): https://doi.org/10.35882/jeeemi.v8i4.1848

simple blink for message acceptance and a double blink for message rejection and retransmission; any non-blink response or an unknown response will not allow the transmission and start a new decoding cycle. In the case of safety-critical outputs, such as breathing problems and medication requests, the notification to the caregiver must occur only after the user has confirmed the message and remains active until the caregiver acknowledges receipt. This read-back, confirmation, and acknowledgment provide closed-loop communication that reduces the likelihood of mistaking a valid message for incorrect. At the same time, this system must be implemented as an auxiliary communication aid, not as an independent emergency or treatment decision-making tool; therefore, no medication or clinical intervention should be performed based on a single decoded message.

The following limitations restrict the application domain of the current results. The system was tested offline in laboratory conditions using healthy volunteers; thus, the presented performance proves its technical viability but cannot be generalized to users with serious problems with speech and movement. Individual differences in voluntary eye movements, involuntary ocular activity, reaction time, and tolerance of multiple blinks may affect the system's performance in clinical conditions [47]. In addition, video verification was conducted by one person, so inter-rater reliability was not calculated. Rest breaks were permitted during data collection, but fatigue was not objectively measured or assessed during the recording session. Nor were end-to-end communication latency, continuous operation, or interactions with caregivers measured. Finally, a fixed vocabulary restricts the ability of the system to produce an infinite number of sentences.

Future research aims to combine current detection and temporal interpretation with machine learning algorithms to identify ambiguous blink responses that are not always solvable with the fixed-threshold decision strategy. The developed hybrid approach will be implemented and validated in real time to improve system robustness and reduce pattern- and message-level errors. Real-time validation will include Arabic visual and speech output, user confirmation, caregiver acknowledgment, end-to-end latency estimation, and testing with target users.

V. Conclusion

In this study, we designed and analyzed an interpretable vertical electro-oculography (EOG) system that encodes 16 predefined Arabic assistive messages via voluntary blinking patterns. The developed framework achieved an F1-score of 95.69% for blink detection, 98.30% macro-F1 for pattern interpretation, and 92.98% accuracy for exact message detection based on 4,000 word-level recordings collected from 25 healthy subjects. These results show the possibility of coding directly at the message level rather than letter-by-letter or in Morse and indicate that errors in decoding individual patterns will propagate throughout the entire four-blink message. However, these findings represent only an offline analysis of healthy controls and cannot demonstrate real-time performance and efficacy for the actual target users. Further research will include applying machine learning in the current process to improve recognition of challenging patterns, after which we will conduct real-time analysis among the target patients. Such testing will need to include individual calibration, latency across the entire process, stability during continuous use, and confirmation from both the patient and the caregiver, particularly for vital messages such as trouble breathing and medication requests.

Acknowledgment

The authors would like to sincerely thank the Department of Computer Engineering, College of Engineering, University of Basrah, for the academic assistance provided throughout this research. The authors would also like to thank all those who volunteered to be part of the EOG recording process and helped in testing the suggested system.

Funding

This research received no specific grant from any funding agency in the public, commercial, or not-for-profit sectors.

Data Availability

The dataset used and analyzed during the current study is inaccessible to the public. Collection of the dataset took place in relation to the current research study only, and the information remains for use exclusively in this research project. It is important that the anonymity of participants is maintained, and thus, the data is not available to any external party.

Author Contribution

Afrah Thamer was involved in conceptualization, methodology design, EOG data collection, signal preprocessing, feature extraction, conducting experiments, result analysis, figures and table creation, and manuscript preparation.
Musaab Alaziz contributed in supervising the research, methodological evaluation, result interpretation, reviewing, and revising the manuscript critically. All authors have read and approved the final manuscript.

Declarations

Ethical approval

Manuscript received 13 May 2026; Revised 20 July 2026; Accepted 30 July 2026; Available online 10 August 2026
Digital Object Identifier (**DOI**): https://doi.org/10.35882/jeeemi.v8i4.1848

This study involving human subjects was approved ethically by the Deanery of the College of Engineering of the University of Basrah, Iraq, as indicated on the Deanery Approval Form. The reference number of this approval form is Ref. No. 20/13/39, while its date is 26 August 2025. The study was approved from 5 September 2025 until 5 September 2027. This approval included non-invasive recording of vertical electrooculography (EOG) signals and video recordings from healthy volunteers to evaluate voluntary single- and double-eye blink recognition, blink pattern interpretation, and decoding messages in Arabic. All the procedures have been conducted according to the approved study protocol, ensuring participant privacy and confidentiality during the experiment.

Consent to Participate

All the subjects gave written informed consents before conducting data collection. Before the recording process, the participants were told about: the study aim; non-invasive EOG recording; placement of surface electrodes around one eye; repetitive voluntary single- and double-blink tasks; usage of video recording only for blink pattern verification purposes; minimum risk associated with possible mild skin discomfort and fatigue; taking rest breaks when needed; and the right to withdraw from the study anytime with no penalty. All the participants have volunteered to be involved in this study.

Consent for Publication

No identifiable participant information, face photos, personal data, or published video materials are included in this manuscript. Anonymized and aggregated research results are presented in this paper. Consent for publication of anonymized research results was given by the participants.

References

[1] Y. Elsahar, S. Hu, K. Bouazza-Marouf, D. Kerr, and A. Mansor, “Augmentative and alternative communication (AAC) advances: A review of configurations for individuals with a speech disability,” *Sensors*, vol. 19, no. 8, Art. no. 1911, 2019, doi: 10.3390/s19081911.

[2] F. Gonçalves, C. S. Fernandes, M. I. Teixeira, C. Melo, and C. Dias, “Bridging silence: A scoping review of technological advancements in augmentative and alternative communication for amyotrophic lateral sclerosis,” *Sclerosis*, vol. 4, no. 1, Art. no. 2, 2026, doi: 10.3390/sclerosis4010002.

[3] A. Tonin, A. Jaramillo-Gonzalez, A. Rana, M. Khalili-Ardali, N. Birbaumer, and U. Chaudhary, “Auditory electrooculogram-based communication system for ALS patients in transition from locked-in to complete locked-in state,” *Scientific Reports*, vol. 10, Art. no. 8452, 2020, doi: 10.1038/s41598-020-65333-1.

[4] G. Chiarion, F. Ponzio, S. Terna, C. Moglia, E. Patti, S. Di Cataldo, and S. Roatta, “e-Pupil: IoT-based augmentative and alternative communication device exploiting the pupillary near-reflex,” *IEEE Access*, vol. 10, pp. 130078–130088, 2022, doi: 10.1109/ACCESS.2022.3229143.

[5] R. Tamai, T. Saitoh, K. Itoh, and H. Zhang, “Eyeglass-type switch: A wearable eye-movement and blink switch for ALS nurse call,” *Electronics*, vol. 14, no. 21, Art. no. 4201, 2025, doi: 10.3390/electronics14214201.

[6] E. Cardillo, L. Ferro, G. Sapienza, and C. Li, “Reliable eye-blinking detection with millimeter-wave radar glasses,” *IEEE Transactions on Microwave Theory and Techniques*, vol. 72, no. 1, pp. 771–779, Jan. 2024, doi: 10.1109/TMTT.2023.3329707.

[7] M. Ezzat, M. Maged, Y. Gamal, M. Adel, M. Alrahmawy, and S. El-Metwally, “Blink-To-Live eye-based communication system for users with speech impairments,” *Scientific Reports*, vol. 13, Art. no. 7961, 2023, doi: 10.1038/s41598-023-34310-9.

[8] M. Thilagaraj, B. Dwarakanath, S. Ramkumar, K. Karthikeyan, A. Prabhu, G. Saravanakumar, M. Pallikonda Rajasekaran, and N. Arunkumar, “Eye movement signal classification for developing human-computer interface using electrooculogram,” *Journal of Healthcare Engineering*, vol. 2021, Art. no. 7901310, 2021, doi: 10.1155/2021/7901310.

[9] G. Ekim, N. Ikizler, and A. Atasoy, “EEG-based communication system by using artificial neural networks,” in *2023 Medical Technologies Congress (TIPTEKNO)*, 2023, pp. 1–4, doi: 10.1109/TIPTEKNO59875.2023.10359177.

[10] M. Rabbani, N. U. S. Sabith, A. Parida, I. Iqbal, S. M. Mamun, R. A. Khan, F. Ahmed, and S. I. Ahamed, “EEG-based real-time classification of consecutive two eye blinks for brain-computer interface applications,” *Scientific Reports*, vol. 15, Art. no. 21007, 2025, doi: 10.1038/s41598-025-07205-0.

[11] C. Belkhiria, A. Boudir, C. Hurter, and V. Peysakhovich, “EOG-based human–computer interface: 2000–2020 review,” *Sensors*, vol. 22, no. 13, Art. no. 4914, 2022, doi: 10.3390/s22134914.

[12] W.-D. Chang, “Electrooculograms for human–computer interaction: A review,” *Sensors*, vol.

Manuscript received 13 May 2026; Revised 20 July 2026; Accepted 30 July 2026; Available online 10 August 2026
Digital Object Identifier (**DOI**): https://doi.org/10.35882/jeeemi.v8i4.1848

19, no. 12, Art. no. 2690, 2019, doi: 10.3390/s19122690.

[13] L. Tao, H. Huang, C. Chen, L. Feijs, J. Hu, and W. Chen, "Review of electrooculography-based human-computer interaction: Recent technologies, challenges and future trends," *Connected Health and Telemedicine*, vol. 2, no. 3, Art. no. 2000010, 2023, doi: 10.20517/chatmed.2023.05.

[14] H. W. Son, T. M. Lee, S. H. Kim, and H. J. Baek, "1D convolutional neural network-based hierarchical classification of eye movements using noncontact electrooculography," *IEEE Access*, vol. 13, pp. 78182–78193, 2025, doi: 10.1109/ACCESS.2025.3566142.

[15] C.-T. Lin, W.-L. Jiang, S.-F. Chen, K.-C. Huang, and L.-D. Liao, "Design of a wearable eye-movement detection system based on electrooculography signals and its experimental validation," *Biosensors*, vol. 11, no. 9, Art. no. 343, 2021, doi: 10.3390/bios11090343.

[16] S. Ban, Y. J. Lee, K. R. Kim, J.-H. Kim, and W.-H. Yeo, "Advances in materials, sensors, and integrated systems for monitoring eye movements," *Biosensors*, vol. 12, no. 11, Art. no. 1039, 2022, doi: 10.3390/bios12111039.

[17] M. Liu, S. Bian, Z. Zhao, B. Zhou, and P. Lukowicz, "Energy-efficient, low-latency, and non-contact eye blink detection with capacitive sensing," *Frontiers in Computer Science*, vol. 6, Art. no. 1394397, 2024, doi: 10.3389/fcomp.2024.1394397.

[18] M. Nyström, R. Andersson, D. C. Niehorster, R. S. Hessels, and I. T. C. Hooge, "What is a blink? Classifying and characterizing blinks in eye openness signals," *Behavior Research Methods*, vol. 56, no. 4, pp. 3280–3299, 2024, doi: 10.3758/s13428-023-02333-9.

[19] A. M. D. E. Hassanein, A. G. M. A. Mohamed, and M. A. H. M. Abdullah, "Classifying blinking and winking EOG signals using statistical analysis and LSTM algorithm," *Journal of Electrical Systems and Information Technology*, vol. 10, Art. no. 44, 2023, doi: 10.1186/s43067-023-00112-2.

[20] D. Das, M. H. Chowdhury, A. Chowdhury, K. Hasan, Q. D. Hossain, and R. C. C. Cheung, "Application specific reconfigurable processor for eyeblink detection from dual-channel EOG signal," *Journal of Low Power Electronics and Applications*, vol. 13, no. 4, Art. no. 61, 2023, doi: 10.3390/jlpea13040061.

[21] J. Xiong, W. Dai, Q. Wang, X. Dong, B. Ye, and J. Yang, "A review of deep learning in blink detection," *PeerJ Computer Science*, vol. 11, Art. no. e2594, 2025, doi: 10.7717/peerj-cs.2594.

[22] K. Suzuki, A. S. M. Miah, and J. Shin, "Deep learning-based eye-writing recognition with improved preprocessing and data augmentation techniques," *Sensors*, vol. 25, no. 20, Art. no. 6325, 2025, doi: 10.3390/s25206325.

[23] N. Zendehdel, K. G. Zadeh, H. Chen, Y. S. Song, and M. C. Leu, "Hands-free UAV control: Real-time eye movement detection using EOG and LSTM networks," *IEEE Access*, vol. 13, pp. 101852–101868, 2025, doi: 10.1109/ACCESS.2025.3578558.

[24] P. Liu, S. Puthusserypady, I. S. MacKenzie, C. Uyanik, and J. P. Hansen, "EarEOG: Using headphones and around-the-ear EOG signals for real-time wheelchair control," *Proceedings of the ACM on Human-Computer Interaction*, vol. 9, no. 3, Art. no. ETRA08, pp. 1–16, 2025, doi: 10.1145/3725833.

[25] A. G. A. Abdel-Samei, A. S. Shaaban, A. M. Brisha, F. E. Abd El-Samie, and A. S. Ali, "EOG acquisition system based on ATmega AVR microcontroller," *Journal of Ambient Intelligence and Humanized Computing*, vol. 14, no. 12, pp. 16589–16605, 2023, doi: 10.1007/s12652-023-04622-9.

[26] X. Ding and Z. Lv, "Design and development of an EOG-based simplified Chinese eye-writing system," *Biomedical Signal Processing and Control*, vol. 57, Art. no. 101767, 2020, doi: 10.1016/j.bspc.2019.101767.

[27] A. M. Choudhari, P. Porwal, V. Jonnalagedda, and F. Mériaudeau, "An electrooculography-based human–machine interface for wheelchair control," *Biocybernetics and Biomedical Engineering*, vol. 39, no. 3, pp. 673–685, 2019, doi: 10.1016/j.bbe.2019.04.002.

[28] S. N. Hernández Pérez, F. D. Pérez Reynoso, C. A. González Gutiérrez, M. de los Á. Cosío León, and R. Ortega Palacios, "EOG signal classification with wavelet and supervised learning algorithms KNN, SVM and DT," *Sensors*, vol. 23, no. 9, Art. no. 4553, 2023, doi: 10.3390/s23094553.

[29] A. J. Molina-Cantero, C. Lebrato-Vázquez, M. Merino-Monge, R. Quesada-Tabares, J. A. Castro-García, and I. M. Gómez-González, "Communication technologies based on voluntary blinks: Assessment and design," *IEEE Access*, vol. 7, pp. 70770–70798, 2019, doi: 10.1109/ACCESS.2019.2919324.

[30] N. Tarek, M. A. Mandour, N. El-Madah, R. Ali, S. Yahia, B. Mohamed, D. Mostafa, and S. El-

Manuscript received 13 May 2026; Revised 20 July 2026; Accepted 30 July 2026; Available online 10 August 2026
Digital Object Identifier (**DOI**): https://doi.org/10.35882/jeeemi.v8i4.1848

Metwally, "Morse glasses: An IoT communication system based on Morse code for users with speech impairments," *Computing*, vol. 104, no. 4, pp. 789–808, 2022, doi: 10.1007/s00607-021-00959-1.

[31] G. Ekim, N. Ikizler, and A. Atasoy, "A study on eye-blink detection-based communication system by using K-nearest neighbors classifier," *Advances in Electrical and Computer Engineering*, vol. 23, no. 1, pp. 71–78, 2023, doi: 10.4316/AECE.2023.01008.

[32] N. Ikizler, G. Ekim, and A. Atasoy, "A novel approach on converting eye blink signals in EEG to speech with cross correlation technique," *Advances in Electrical and Computer Engineering*, vol. 23, no. 2, pp. 29–38, 2023, doi: 10.4316/AECE.2023.02004.

[33] I. Käthner, A. Kübler, and S. Halder, "Comparison of eye tracking, electrooculography and an auditory brain-computer interface for binary communication: A case study with a participant in the locked-in state," *Journal of NeuroEngineering and Rehabilitation*, vol. 12, Art. no. 76, 2015, doi: 10.1186/s12984-015-0071-z.

[34] K. S. Moon, S. Q. Lee, J. S. Kang, A. Hnat, and D. B. Karen, "A wireless electrooculogram (EOG) wearable using conductive fiber electrode," *Electronics*, vol. 12, no. 3, Art. no. 571, 2023, doi: 10.3390/electronics12030571.

[35] H. N. Jo, S. W. Park, H. G. Choi, S. H. Han, and T. S. Kim, "Development of an electrooculogram (EOG) and surface electromyogram (sEMG)-based human computer interface (HCI) using a bone conduction headphone integrated bio-signal acquisition system," *Electronics*, vol. 11, no. 16, Art. no. 2561, 2022, doi: 10.3390/electronics11162561.

[36] H. Liu, H. Wei, G. Yang, C. Xia, and S. Zhao, "An improved ViBe algorithm based on adaptive thresholding and the deep learning-driven frame difference method," *Electronics*, vol. 12, no. 16, Art. no. 3481, 2023, doi: 10.3390/electronics12163481.

[37] B. Voloh, M. R. Watson, S. König, and T. Womelsdorf, "MAD saccade: Statistically robust saccade threshold estimation via the median absolute deviation," *Journal of Eye Movement Research*, vol. 12, no. 8, Art. no. 3, 2019, doi: 10.16910/jemr.12.8.3.

[38] Z. Yang, L. Hou, and X. Zhao, "Robust autocorrelation for period detection in time series," in *Proceedings of the 17th International Conference on Agents and Artificial Intelligence (ICAART), Volume 2*, Porto, Portugal, 2025, pp. 36–44, doi: 10.5220/0013092500003890.

[39] W.-D. Chang, H.-S. Cha, K. Kim, and C.-H. Im, "Detection of eye blink artifacts from single prefrontal channel electroencephalogram," *Computer Methods and Programs in Biomedicine*, vol. 124, pp. 19–30, Feb. 2016, doi: 10.1016/j.cmpb.2015.10.011.

[40] B. F. Händel, X. Chen, M. Inbar, F. Kusnir, and A. N. Landau, "A quantitative assessment of EOG eye tracking during free viewing in sighted and congenitally blind individuals," *Brain Research*, vol. 1864, Art. no. 149794, 2025, doi: 10.1016/j.brainres.2025.149794.

[41] A. Vince, "A combinatorial approach to binary positional number systems," *Acta Mathematica Hungarica*, vol. 143, no. 1, pp. 138–158, 2014, doi: 10.1007/s10474-013-0387-8.

[42] O. Rainio, J. Teuho, and R. Klén, "Evaluation metrics and statistical tests for machine learning," *Scientific Reports*, vol. 14, Art. no. 6086, 2024, doi: 10.1038/s41598-024-56706-x.

[43] C. Miller, T. Portlock, D. M. Nyaga, and J. M. O'Sullivan, "A review of model evaluation metrics for machine learning in genetics and genomics," *Frontiers in Bioinformatics*, vol. 4, Art. no. 1457619, 2024, doi: 10.3389/fbinf.2024.1457619.

[44] K. Kleifges, N. Bigdely-Shamlo, S. E. Kerick, and K. A. Robbins, "BLINKER: Automated extraction of ocular indices from EEG enabling large-scale analysis," *Frontiers in Neuroscience*, vol. 11, Art. no. 12, 2017, doi: 10.3389/fnins.2017.00012.

[45] R. Zargari Marandi, P. Madeleine, Ø. Omland, N. Vuillerme, and A. Samani, "Eye movement characteristics reflected fatigue development in both young and elderly individuals," *Scientific Reports*, vol. 8, Art. no. 13148, 2018, doi: 10.1038/s41598-018-31577-1.

[46] Y. Ding, P. Tang, J. Li, C. Zeng, Y. Sun, Y. Zhang, and W. Liu, "Study for electrooculography character input based on dual-channel CNN of movement disorder patients," *IEEE Access*, vol. 12, pp. 101865–101877, 2024, doi: 10.1109/ACCESS.2024.3432130.

[47] C. Verbaarschot, D. Tump, A. Lutu, M. Borhanazad, J. Thielen, P. van den Broek, J. Farquhar, J. Weikamp, J. Raaphorst, J. T. Groothuis, and P. Desain, "A visual brain-computer interface as communication aid for patients with amyotrophic lateral sclerosis," *Clinical Neurophysiology*, vol. 132, no. 10, pp. 2404–2415, Oct. 2021, doi: 10.1016/j.clinph.2021.07.012.

Manuscript received 13 May 2026; Revised 20 July 2026; Accepted 30 July 2026; Available online 10 August 2026
Digital Object Identifier (**DOI**): https://doi.org/10.35882/jeeemi.v8i4.1848

Journal of Electronics, Electromedical Engineering, and Medical Informatics
Homepage: jeeemi.org; Vol. 8, No. 4, October 2026, pp: 1331-1353 **e-ISSN: 2656-8632**

Author Biography

Afrah Thamer received her BSc. degree in Computer Engineering from the College of Engineering, University of Basrah, Basrah, Iraq, in 2021. She is currently pursuing the MSc. degree in Computer Engineering at the same university. Her MSc. research focuses on vertical electrooculography (EOG) signal processing for voluntary eye-blink detection and Arabic assistive communication. Her research interests include biomedical signal processing, EOG-based human–computer interaction, wearable assistive technologies, and machine learning for biomedical applications. Email: afrah.dhamid@uobasrah.edu.iq.

Musaab Alaziz Holds a PhD in degree in Electrical and Computer Engineering from Rutgers University, the state university of New Jersey, NJ, USA in 2017. MSc, BSc in Computer Engineering from University of Basrah, Basrah, Iraq in 2005 and 2002 respectively. He is currently a faculty member at University of Basrah, College of Engineering and Head of the Computer Engineering Department at the same college. His research interests include unobtrusive monitoring and neurobehavioral assessment and computational modeling. He recently carried out a research project on smart rooms that can track people's activities using sensors with smart systems. Email: mosab.adil@uobasrah.edu.iq

Manuscript received 13 May 2026; Revised 20 July 2026; Accepted 30 July 2026; Available online 10 August 2026
Digital Object Identifier (**DOI**): https://doi.org/10.35882/jeeemi.v8i4.1848